Hindawi
Journal of Chemistry
Volume 2023, Article ID 9780955, 24 pages
https://doi.org/10.1155/2023/9780955

Review Article

Recent Advances in Efficient Photocatalytic Degradation Approaches for Azo Dyes

Arpita Paul Chowdhury,[1] **K. S. Anantharaju**,[1] **K. Keshavamurthy**,[2] **and Samuel Lalthazuala Rokhum**[3]

[1]*Department of Chemistry, Dayananda Sagar College of Engineering, Bengaluru 560078, India*
[2]*Department of Physics, Dayananda Sagar College of Engineering, Bengaluru 560078, India*
[3]*Department of Chemistry, National Institute of Technology, Silchar 788010, Assam, India*

Correspondence should be addressed to Samuel Lalthazuala Rokhum; rokhum@che.nits.ac.in

Received 4 September 2023; Revised 15 November 2023; Accepted 7 December 2023; Published 26 December 2023

Academic Editor: Kamala Kanta Nanda

In recent decades, the textile industry has contributed to continuous pollution in the environment. Synthetic dyes which are commonly found in waste water are azo, sulfur, anthraquinone, triphenylmethyl, indigoid, and phthalocyanine derivatives. These pollutants block the light penetration in water bodies and prevent photosynthesis activity, thereby affecting aquatic life. As an environmental crisis, several technologies have been explored to control pollution. Among all the techniques, the photocatalysis process is considered as a green, simple, and economical process. To improve the photocatalytic activity, researchers worldwide have investigated various photocatalysts such as metal oxides, metal ferrites, and heterostructured nanocomposites. The major goal of this review article is to propose a high-performing, cost-effective hybrid photocatalyst reported to date for prospective azo dye pollutant remediation. This review article also aimed to highlight the challenges and uncertainties associated with dye degradation in the photocatalytic process.

1. Introduction

Industrialization growth worldwide drastically leads to environmental problems due to release of the pollutants. According to the reports, about 20% of the total production of dyes is being discharged into the water surface [1]. These toxic chemicals cause great concern for both the environment and public health. The extreme discharge of the effluent adversely affects aquatic life and soil fertility and disturbs the ecosystem integrity by increasing the chemical oxygen demand and biochemical oxygen demand, altering the pH, and affecting water quality [2]. The wastewater containing organic dye pollutants blocks the ecosystem and causes threats to environmental sustainability. The intense color of the wastewater discharges due to the textile dyeing industry cannot be hidden, which is persistent due to the poor biodegradability of these dyes [3]. Dyes absorb the visible spectrum light from 380 to 750 nm. The dye molecule consists of three essential groups: the chromophore, the auxochrome, and the matrix. The chromophore is the active site of the dye in which upon excitation, the electrons of a molecule absorb light energy. Chromophore-containing molecules feature extensively in surgical practice, with synthetic dyes gaining popularity over endogenous optical adjuncts [4]. The common chromophore are $-NO_2$, $-N=N-$, $-C=S$, $-C=O$, $-C=C-$, and $-N=O$. The organic molecules containing these groups are known as chromogenic. The chromogenic molecule with the accumulation of auxochrome groups shows dyeing possibilities. These auxochrome groups allow the fixation of the dyes and can modify the color of the dye. The auxochrome groups are acidic (COOH, SO_3, and OH) or basic (NH_2, NHR, and NR_2), while the third part of the molecule is the rest part of the atom called as matrix [5]. The azo dyes with the (-N=N-) chromophore group account for 70% market share and are highly soluble in water [6].

The nitro group presence makes the dye mutagenic and highly toxic. The breakdown products, such as 1,4-phenylenediamine and o-tolidine, are highly poisonous [7]. However, the main limitation of these dyes is their potential carcinogenicity which limits its application [8]. Recent documentation has found an interplay of azo dyes with human serum albumin and hemoglobin [9]. Consequently, the elimination and prior treatment of this colored pollutant are essential and challenging. Many technologies have emerged for the treatment of polluted water. The treatment methods such as the membrane process, biological process, reverse osmosis, chemical and electrochemical technology, ion exchange, electrodialysis, electrolysis, adsorption techniques, and advanced oxidation processes are commonly used in conventional treatment technologies [10]. These methods are not efficient to completely destruct the chromophoric structure of the dye. Advanced oxidation processes (AOPs), such as the photocatalytic degradation process recently considered as an eco-friendly, cost-effective, and complete mineralization of the dyes are observed compared to traditional methods. The active radicals such as hydroxyl radicals (•OH), superoxide anion ($\bullet O_2^-$), and hydrogen peroxide (H_2O_2) are generated in situ to degrade organic dye compounds [11]. Thus, photocatalysis is a greener way to debase the pollutants of water with semiconductors and is intensely investigated worldwide [12].

The objective of this present review article is to explore applications of different nanomaterials as a robust photocatalyst for the treatment of wastewater containing azo dyes generated from textile industries. In particular, the authors focussed on the recent developments and included studies only published in the years, 2015–2023. Additionally, the effect of different parameters which includes the dye concentration effect of light irradiation, pH, and catalyst loading is discussed for the optimization of the degradation efficiency of textile wastewater.

2. Chemical Structure and Classification of Azo Dyes

The chemical structure of an azo dye, in general, consists of a solubilizing group, auxochrome groups, and chromophoric groups [13]. The structure of an azo dye is depicted in Figure 1. The nature of the azo bonds and the associated chromophore and auxochrome groups decide the color of the dyes. The number of azo linkages present in an azo dye molecule classifies the molecule as monoazo, diazo, triazo, and polyazo. Furthermore, azo dyes can be subdivided into acidic, basic (cationic), direct (substantive), disperse (nonionic), reactive, vat, and sulfur dyes [14]. Azo dyes in the color index (CI) system are categorized with numbers that range from 11,000 to 39,999 in correspondence with the chemical structure [15–17]. Figures 2 and 3 illustrate the classification of the dyes.

3. Dye Removal Technologies

The dyes containing waste from the textile industries need to be treated to remove the pollutants for the safety of the marine environment and ecosystem. Many technologies have emerged for the remediation of these dyestuffs. The treatment technologies are broadly classified as (a) biological treatment, (b) physicochemical treatment, (c) advanced approaches, and (d) combinatorial treatment [18]. Figure 4 represents the overview of different dye removal technologies.

3.1. Biological Treatment. Biological treatment is a low-cost and effective method for azo dye removal. The azo bond cleavage is difficult under the aerobic condition, but in the anaerobic condition, it can be easily accomplished. At present day, the technology comprising the anaerobic and aerobic conditions is used to degrade azo dye wastewater [19].

3.1.1. Fungal-Assisted Degradation. Fungi are present everywhere in the natural ecosystem, and it has a strong ability to adopt metabolism to various carbon and nitrogen sources. Recent studies reported that complex organic pollutants can be degraded in the presence of fungi by secreting various intracellular and extracellular enzymes [20]. The decolorization of azo dyes by fungi is triggered by adsorption onto hyphae, followed by the breakage of chemical bonds through extracellular enzymes [21]. Various reports have been published that showed fungal biomass possesses the potential to degrade and decolorize a wide variety of azo dyes. Gomaa et al. [22] explored *Aspergillus arcoverdensis* SSSIHL-01 fungi for the removal of CR dye and reported 98.6% efficiency. Ali et al. [23] used *Meyerozyma caribbica* SSA1654 and showed biodegradation of Acid orange 7 dye. Pulp wash was used to synthesize *Pleurotus sajor-caju*-fungal lignin-modifying enzymes for an inducing substrate, and for cell immobilization, *L. cylindrica* (L.C) was used. The fungus showed higher Lac activity (126.5 $IU \cdot mL^{-1}$) and was used for RB 5 decolorizing of the dye with 89.4% decolorization as demonstrated by Fernandes et al. [24].

3.1.2. Yeast Assisted. Yeasts have great capability for bioremediation of xenobiotics deposited in wastewater. However, only a few reports are present so far that deal with the biodegradation of aromatic dye pollutants [25, 26]. *Pichia occidentalis* A2, a halotolerant yeast, was recently reported by Wang et al. [27] that can degrade acid red B azo dye. The CR dye with 100% efficiency was successfully removed by the adsorption process step with brewery yeast reported by Soh et al. [28]. Yeast consortium *Meyerozyma guilliermondii*, *Yarrowia* sp., and *Sterigmatomyces halophilus* showed degradation of RR 120 as demonstrated by Ali et al. [29].

3.1.3. Algal- and Bacterial-Assisted Degradation. The potential cyanobacteria, Rotifera, and Cercozoa can show AO-2 biodegradation with 95% efficiency demonstrated by Zhang et al. [30]. The study was conducted by Hamouda et al. [31] to explore the green microalga *Scenedesmus obliquus* growth using a disperse orange 2RL azo dye. After 7 days of algal growth with dye, the highest decolorization of

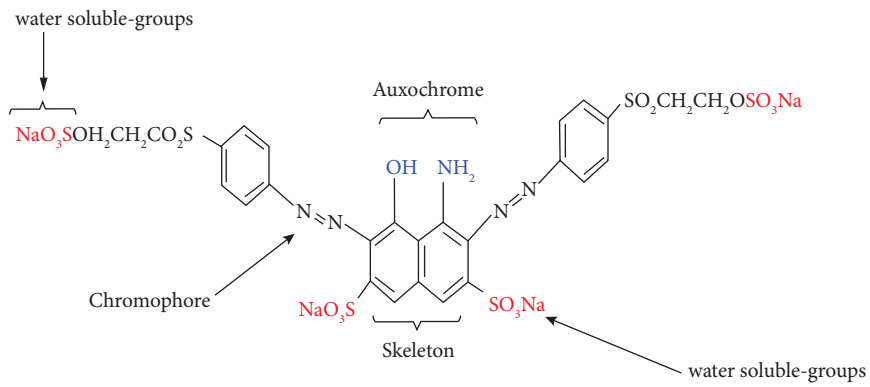

Figure 1: Azo dye chemical structure, reproduced from reference [13] (copyright 2020, with permission from Elsevier).

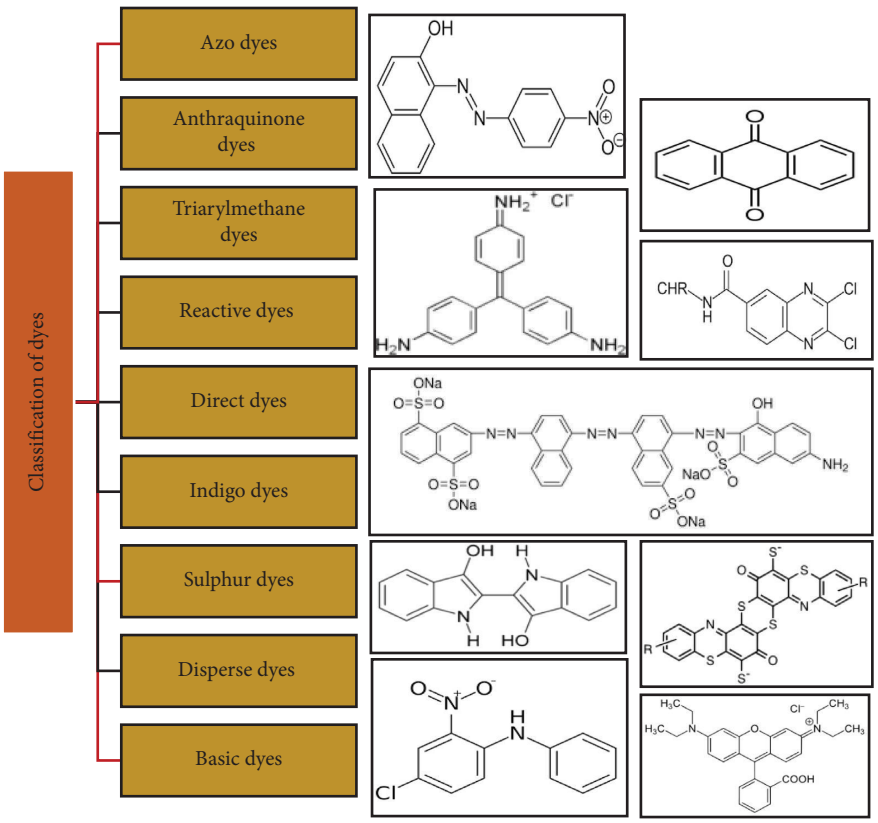

Figure 2: Classification of dyes with chemical structure.

dispersed orange 2RL azo dye (98.14%) was observed. El-Sheekh [32] reported *Chlorococcum* sp. for the elimination of reactive orange 2RL and reactive red M-2BF azo dye. At 40 ppm for reactive orange 2RL and 20 ppm for reactive red M-2BF, maximum decolorization was obtained. Agarwal et al. [33] developed a biofilm reactor for the decolorization of dyes. The reactor was continuously operated for 264 days, achieving a ≥96% reduction in COD and ADMI values. The study highlighted by Patel and Gupta [34] for the dye decolorization of acid maroon V by a potential bacterial consortium EDPA containing *Enterobacter dissolvens* AGYP1 and *Pseudomonas aeruginosa* AGYP2 in the presence of redox mediators.

3.2. Phytoremediation. The scientific community focussed on the alternative eco-friendly technique for the remediation of toxic dye wastage accumulated in soil and water bodies. It is considered as a sustainable alternative method for carrying out needed degradation [35]. Plant species such as *Phaseolus mungo*, *Sorghum vulgare*, and *Brassica juncea* have been evaluated for decolorization. Wetlands decolorization obtained by cocoyam plantations is 72%–77% efficient. *Tagetes patula* L. root system can efficiently degrade the reactive orange M2RL, reactive red M5B, methyl red, MO, and navy blue HE2R dyes [36, 37]. Though biological treatment is efficient, it is considered less flexible in design and operation. Moreover, satisfactory color removal and mineralization are

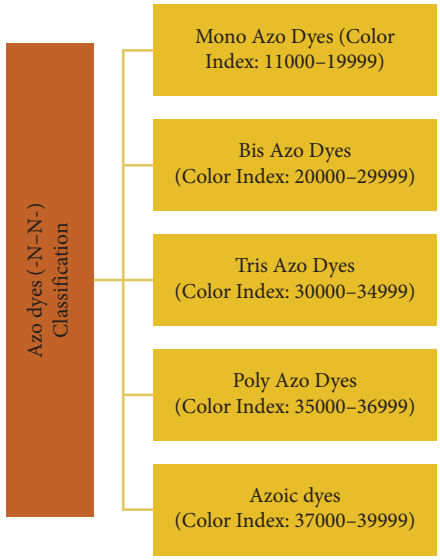

Figure 3: Classification of azo dyes, reproduced from reference [17] (copyright 2022, with permission from Elsevier).

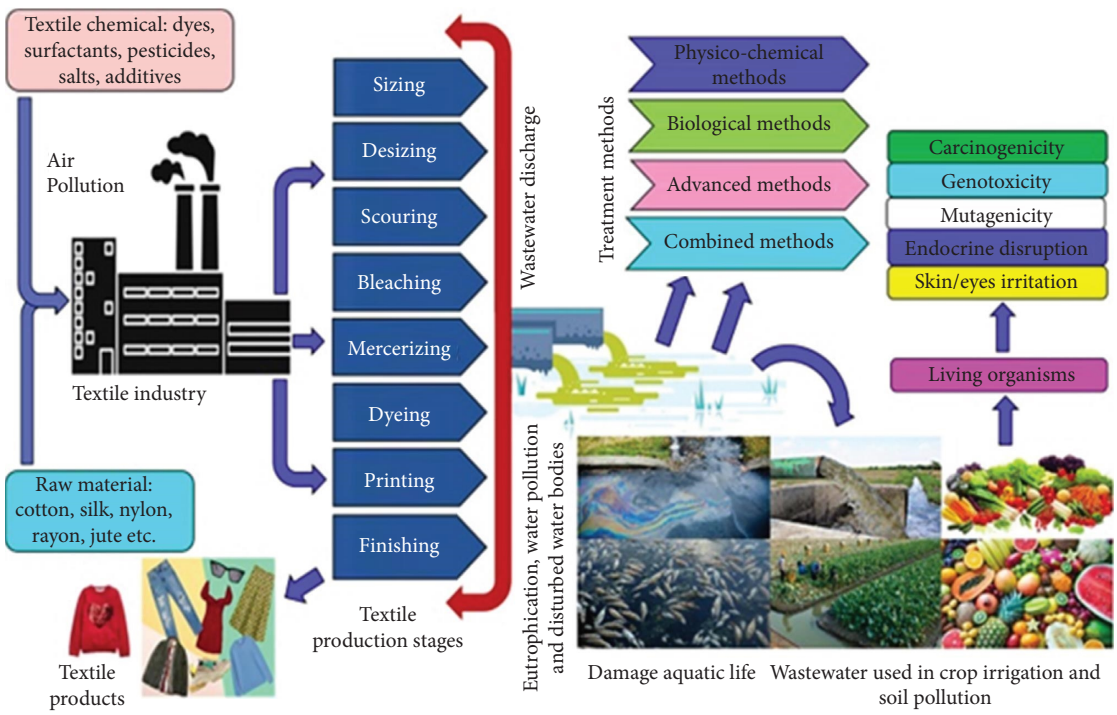

Figure 4: Water treatment technologies, reproduced from reference [18] (copyright 2021, with permission from Elsevier).

not achieved. The complex chemical structure due to xenobiotic nature the biodegradability of azo dyes are limited [38]. However, in the anaerobic condition, it usually generates aromatic amines, which possess high biotoxicity and cannot be completely degraded. Hence, efficient and effective treatment processes need to be developed for the complete removal of azo dyes from wastewater [39].

3.3. Physicochemical Treatment. Physicochemical treatment is a separation technique that involves chemical reaction and includes processes such as the addition of coagulant, adsorption studies, chemical oxidation, flocculation, and electrocoagulation. Some of the processes are discussed as follows.

3.3.1. Adsorption. Adsorption is a surface phenomenon, in which only the adsorbent surface is concerned, and adsorbate should not penetrate inside the structure of the adsorbent [40]. Adsorption can be classified as physical adsorption and chemical adsorption. In physical adsorption, weak electrostatic forces bind the adsorbate to the adsorbent surface, and in chemisorption, strong covalent bonds exist between the adsorbate and adsorbent surfaces [41, 42]. The advantages of the adsorption process include the reusability of adsorbents, high efficiency, and the short time required for dye removal from wastewater [43]. Recently, He et al. [44] synthesized activated carbon based on edamame shell for the effective adsorption and removal of CR dye. Graphene oxides-TiO_2 is synthesized by Cano et al. [45] through the ball milling process. Efficient adsorption for methylene blue dye is observed within 9 min. Wang et al. [46] designed $CoFe_2O_4$/chitosan magnetic adsorbent supported on Mxene for the removal of CR, RhB, and MG dyes. The adsorption capacity for CR dye is up to 2095.9 $mg{\cdot}g^{-1}$. In another work, Ti-MOFs were reported by Zhao and his coworkers [47] for the adsorption of methylene blue, methyl orange, and indigo dyes. Rana and Sharma [48] fabricated Fe_3O_4 embedded oxidized Sterculia gum/Gelatin hybrid and evaluated for the enrichment of MO and MB with maximum adsorption of 90% and 88%, respectively. Qasem et al. [49] reported Co-MOF@CNT nanocomposite for adsorption of cationic dye with 98% removal of MB dye at neutral pH. MnO_2-NP-CPC efficient adsorbent synthesized by Belcaid et al. [50] was analyzed for the removal of three different toxic dyes. In the same line, Sudan et al. [51] synthesized biochar from rice husk and investigated the adsorption of EBT dye and found 94% removal within 2 h contact time at 1.5 g catalyst dosage.

3.3.2. Ion Exchange. The ion exchange process significantly removes dyestuffs. The ion exchange resin has capability to disperse in concentrate contaminants [52]. Ion exchange resins have been classified based on the charge of the exchangeable counter ion and the ionic strength of the bound ion. Ion exchange resins are classified as (a) strong cation-exchange resins ($—SO_3\text{-}H^+$), (b) weak cation-exchange resins ($—COO\text{-}H^+$), (c) strong anion exchange resins of quaternary ammonium groups (type I resins contain $—CH_2N(CH_3)_3{}^+Cl^-$ groups and type II resins contain $—CH_2N(CH_3)_2(CH_2CH_2OH)^+Cl^-$ groups), and (d) weak anion exchange resins of primary ($\text{-}NH_2$), secondary (=NH), or tertiary-amine (≡N) functional groups in the chloride or hydroxide form [53]. Lu et al. [54] reported the magnetic cation-exchange microbeads for the removal of CV and acid green 9 dye. Cellulose films were grafted with p(GMA) via the ATRP method, and the epoxy groups were converted into phosphate (RCF-g-p(GMA)-PO_3H_2) and sulfate (RCF-g-p(GMA)-SO_3H) groups and used for the removal of chlorazole Black E by Bayramoglu and Arica [55]. In the meantime, Marin et al. [56] used the resin amberlite IRA 400, a basic anionic exchange resin for the treatment of acid orange 7. The sorption capacity at 25°C and 65 min was 317.6 $mg{\cdot}g^{-1}$. The ion exchange behavior of microsized ammonium phosphomolybdate (APM) was investigated by Joseph and his coworkers [57] for the removal of MB, EY, MG, and MR dyes.

3.3.3. Coagulation and Flocculation. Coagulation-flocculation is a low capital cost, simple operation and is widely used for dye removal without the formation of any secondary pollutants. In this process, the dye solution system is destabilized to form agglomerates or flocs which settle down under gravity [58]. It is a well-known process, and here, with the addition of a coagulant, destabilization of the colloidal particles is carried out. The various operational factors are colloidal characteristics, turbidity, alkalinity, pH, and colloidal [59]. Hadadi et al. [60] in their research demonstrated *Pinus halepensis* Mill. seed extract' biocoagulant efficacy for treating Congo red-containing wastewater. Around 80% dye removal with coagulant dosages from 3 to 12 $mL{\cdot}L^{-1}$ is achieved. In the current investigation, Shende and his coworkers [61] have found that synthetic dyes MO, CR, MB, and safranin were removed from wastewater by cocoyam bioflocculant. The electrostatic force of attraction and hydrogen bonding mechanisms were observed for the dye removal process. The work by Ihaddaden et al. [62] reported the use of bentonite and *Opuntia ficus-indica* as coagulant-flocculant for the MB dye removal. The dye removal efficiency obtained is 98.29% within 19 min. Duan et al. [63] studied the removal of reactive orange using magnesium hydroxide and polyacrylamide and described the coagulation performance and floc characteristics. Obiora-Okafo et al. [64] explored natural organic polymers, *Brachystegia eurycoma* coagulant, and *Vigna subterranean* coagulant for the decolorization of AR44 found in wastewater. The kinetics of the coagulation-flocculation process was confirmed to be a pseudo-second-order model with $R^2 > 0.997$.

3.3.4. Membrane Filtration. Membranes have been used in several studies to treat colored wastewater and are considered one of the best solutions to clean wastewater due to their high separation efficiency, reliability, cost-effectiveness, and simplicity. Thus, ultrafiltration, nanofiltration, and microfiltration are an attractive technology. Polymeric materials, for example, PES, PAN, PVDF, and BPPO, are efficiently used [65, 66]. Li et al. [67] in their research reported MXene-PANI/PES membrane for CR and MB dyes removal [67]. Yusaf et al. [68] employed micellar-enhanced ultrafiltration for the removal of Procion blue MxR. Subrahmanya and his coworkers [69] reported a syringe filter membrane composed of Whatman 42 filter, GO_{10}/(SBA-15/PDA)$_2$ membrane to effectively screen MB and EBT dyes from wastewater. PVDF/IL-Na^+MMT membrane is fabricated by Zhao et al. [70] for removal efficiency for both

anionic and cationic dyes at a high level of over 90% efficiency. Li et al. [71], in their study, prepared a novel antifouling loose nanofiltration (LNF) membrane by cross-linking and grafting of hydrolyzed polyacrylonitrile ultrafiltration substrate with a PEI-based zwitterionic polymer PEI-CA through the covalent amide bond for the treatment of dye brilliant blue R, CR, MB, and chrome black T. Dmitrenko et al. [72] reported PAN membranes by various TiO_2 modifications [72]. Nanofiltration is a separation technology, where pore size ranges about 0.5–2.0 nm with molecular weight cutoff ranging from 200 to 2000 Da. The smaller pore size, higher permeability, and lower transmembrane pressure are advantages over ultrafiltration and microfiltration. Recently, Ahmadipouya et al. [73] reported polysulfone mixed-matrix nanofiltration membranes containing UiO-66 metal-organic framework and incorporated for MG, MB, MO, and MR dye adsorption. Li et al. [74] in their work prepared the antibacterial NF membrane using a hydrophilic antibiotic streptomycin with trimesoyl chloride for desirable performance for excellent dyes rejections such as DR 23, CR, AR66, Victoria blue B, and chrome black T dyes.

Nevertheless, the physicochemical process is not considered suitable for wastewater treatment due to its high costs and low efficiency. Moreover, disposal problems of the secondary waste generated which gets converted into toxic intermediates.

3.4. Advanced Approaches

3.4.1. Ozonization. Ozonation technology is a chemical oxidation treatment affected with ozone which possesses a strong ability to remove color and smell and is widely used for the treatment of wastewater. Li et al. [75] investigated the ozonization process on reactive dyes such as reactive blue FL-RN, reactive red FL-2BL, and reactive yellow FL-2RN. The synthetic azo dye, reactive black 5, and ozonization were probed by Chu et al. [76] with a microbubble generator. The catalytic ozonation reaction by Ru impregnated on SBA-15 material as a catalyst for reactive orange 4 was reported by Ghuge and Saroha [77]. Le et al. [78] in his work studied the decolorization of reactive red 239 and DB 71 using an ozonation membrane contactor containing PVDF. Fe-RGO oxidation catalyst is prepared by Qazi et al. [79] to investigate the ozonization process for the removal of MB dye by catalytic ozonation at pH 7. The catalyst dose was 0.02 g, and the ozone dose was 0.5 mg/min. Around 96% removal efficiency was achieved after 10 min. Dabuth and his coworkers [80] reported a catalyst consisting of coconut and coal-based activated carbon and eucalyptus biochar coated by titanium dioxide for catalytic ozonation. It is reported that the ozonation technique in wastewater dye pollutant removal is effective, but the complete mineralization of organic substances is still a challenge.

3.4.2. Electrocoagulation. The electrocoagulation technique is a simple, reliable, and low-cost method for the treatment of dyes contained in wastewater. The process has good removal efficiency for COD, color, turbidity, and dissolved solids. The advantage of electrocoagulation over coagulation is the use of fewer reagents, lower conductivity, and neutral pH value, which suits the treated water for some industrial applications [81]. In this technique, a direct current source is applied between metal electrodes, which produces metal hydroxides immersed in polluted water. The metal hydroxides formed lead to the removal of the contaminants by acting as coagulants [82]. A study by Márquez et al. [83] deals with electrocoagulation techniques for the removal of brilliant green dye. The electrocoagulation process investigated by Lach et al. [84] revealed a high azo dye removal efficiency (96.5%) with TOC and COD of 93.5% and 85.0%, respectively. Liu et al. [85] presented a reverse electrocoagulation treatment of methyl orange and alizarin yellow dyes using Fe-Fe electrodes. The efficiency for methyl orange and alizarin yellow achieved was 98.7% and 98.6%, respectively, using NaCl as the electrolyte. Yao et al. [86] designed an electrocoagulation reactor and studied methyl orange as the target pollutant and found 92.16% removal efficiency with 16.8% COD removal efficiency. Brilliant yellow azo dye removal by the electrocoagulation method was reported by Ahmed et al. [87] using an Al helical coil and obtained 92% efficiency in dye removal within 90 min. Handaoui et al. [88] reported indigo dye removal with 98.4% removal at a pH of 7.5 and in 60 mg/L solution concentration. The electrocoagulation is an eco-efficient electrolysis-based technology, but the electrodes need to be replaced which is a disadvantage and may also lead to electrode passivation [89].

3.4.3. Fenton Oxidation. The Fenton oxidation is an advanced alternative process for the treatment of textile azo dyes. The Fenton reaction process involves the reaction between hydrogen peroxide and iron which further produces reactive oxygen and hydroxyl species that enhance the degradation of pollutants in the absence or presence of light (photo-Fenton) [90]. Eskikaya et al. [91] studied the degradation of BR18 and RR180 using the hydrochars obtained from laurel leaves and watermelon peels and observed removal efficiency of 98.8% and 99.8% within 60 min and with 100 $mg \cdot L^{-1}$ initial dye concentration. Magnetic Fe_3O_4-NIO calcium alginate beads were prepared by Ayed et al. [92] for the degradation of Novacron blue dye. The researcher observed 80% efficiency in the photo-Fenton process compared to only the Fenton process (50%) after 120 min reaction time. Jain et al. [93] fabricated zinc oxide-graphene oxide nanohybrid and employed it for brilliant green degradation. Tang et al. [94] prepared Cu-FeOOH/TCN composites and acquired 97.8% degradation efficiency with an 85.5% mineralization rate. The $SrWO_4$@MIL-88A(Fe) composites were reported by Wei et al. [95] for the degradation of MB within 4 min and 93.75% degradation rate was achieved. Dai et al. [96] synthesized ferrous ion-modified Laponite@diatomite composite for photo-Fenton degradation of MO and obtained a degradation rate of 99% in 240 min.

Though Fenton oxidation is an effective technology, it is limited to large-scale applications due to the excessive iron

sludge production and formation of toxic secondary by-products.

3.4.4. Nanophotocatalysis. The researchers to date focussed on various conventional approaches for the remediation of harmful chemical contaminants. These approaches are time-consuming and very costly, and their usage has been limited. Recently, nanotechnology emerged as an efficient, clean, and environmentally benign alternative technique originating from the unique properties of nanomaterials. The nanophotocatalysis process has an advantage, and it is a powerful way to clean up the extremely noxious and stable molecules from the environment and has received much attention due to its low cost, high efficiency, and low toxicity [97]. In 1938, TiO_2 was discovered by Goodeve and Kitchener [98] for bleaching of dyes in the presence of O_2. Since then, scientists have been keen on investigating the fundamental principles in photocatalysis reactions and continuous search for new efficient photocatalysts. In the photocatalysis phenomenon, a semiconductor is capable of conducting electricity in the presence of light at room temperature. The photocatalyst provides a site for both oxidation and reduction reactions simultaneously for the mineralization of pollutants [99].

3.4.5. Principle of the Photocatalytic Oxidation Process. The mechanism of photocatalysis can be described by the following four important steps: (i) generation of electron-hole pairs, (ii) excited charges separation, (iii) migration of photogenerated electrons and holes to the surface of photocatalysts, and (iv) redox reactions. The holes oxidize the pollutant-containing water molecules and produce hydroxyl radicals, and electrons reduce the dissolved oxygen in water to produce superoxide anion [100]. The main processes and key reactions involved in nanophotocatalysis are presented in Figure 5.

The photocatalysis reaction can be categorized as homogeneous photocatalysis and heterogeneous photocatalysis [102].

(1) Homogeneous Photocatalysis. Here, both the reactants and catalyst are uniformly distributed in the same phase. The molecular catalysts, catalytic sites for oxidation and reduction processes, are all in a solution form. The ozone and photo-Fenton systems are the most used homogeneous photocatalysis systems. The reactive species is $OH^{\bullet}$, which is used for various purposes.

(2) Heterogeneous Photocatalysis. In heterogeneous photocatalysis, the photocatalyst is in contact with aqueous organic compounds or pollutants. Here, the reactant species are present in different physical states. The semiconductor-mediated heterogeneous photocatalysis is generally preferred because of its easy separation of the catalysts, energy-efficiency, and mild reaction conditions. Considerable efforts have been placed on the design and fabrication of heterojunctions for improving photocatalytic activity. Based on the interface of the different materials, the heterojunction photocatalysts are categorized into four steps: (i) the semiconductor-semiconductor (abbreviated as S-S) heterojunction; (ii) the semiconductor-metal (abbreviated as S-M) heterojunction; (iii) the semiconductor-carbon group (abbreviated as S-C) heterojunction (carbon group: activated carbon, carbon nanotubes (CNTs), and graphene); and (iv) multicomponent heterojunction [103].

In semiconductor-based composites, the charge may migrate from one component, typically the semiconductor absorbing irradiation to the other component, with proper band-edge positions. Reasonably, a composite photocatalyst system, composed of one semiconductor as the light absorber and other components to enhance the photocatalytic processes, is supposed to be an effective prototype to overcome the above shortcomings. Moreover, the second or third component in the composites may also provide active centers for the activation of reactants for the subsequent reduction/oxidation reactions, by working as a cocatalyst.

3.4.6. Basics of Heterojunction. The heterojunction is defined as the interface between two different semiconductors with unequal band structure. The internal structure of semiconductors comprises some band alignments which act as the basis for the formation of heterostructures. Based on the alignment of energy levels, heterostructures/heterojunction can be categorized into three types: (a) straddling type, (b) staggered type, and (c) those with a broken gap, as shown in Figure 6 [104].

In straddling type heterojunctions (type I), semiconductor A has a wider energy band gap than B. This results in the accumulation of the charge carriers on the semiconductor with a smaller band gap, and so, recombination of charge carriers is still possible since both electrons and holes are accumulated on the same semiconductor. In staggered-type heterojunction (type II), the VB and CB of semiconductor A are higher and lower than those of B. This results in the spatial separation of charge carriers which prevents the recombination of electrons and holes. The broken gap (type-III heterojunction) is the same as the staggered type except that the staggering gap becomes so wide that electron-hole migration is not possible, and therefore, the separation cannot occur [105–107]. Another, new Z-scheme photocatalyst is identified from the natural photosynthesis process. In this mechanism, two semiconductor photocatalysts are connected, an oxidation photocatalyst and another is reduction photocatalyst (Figure 7) [108].

The low VB position of the oxidation photocatalyst and high CB position of reduction photocatalysts are usually found in the *Z*-scheme photocatalyst. The strong reduction ability of photogenerated electrons in the CB of photocatalyst 1 and oxidation abilities in the VB of PC II are observed. Thus, a *Z*-scheme photocatalyst simultaneously has a strong redox ability.

4. Photocatalytic Degradation of Azo Dyes

The advanced oxidation processes (AOPs) are able to deal with the problem of dye destruction in aqueous systems. In

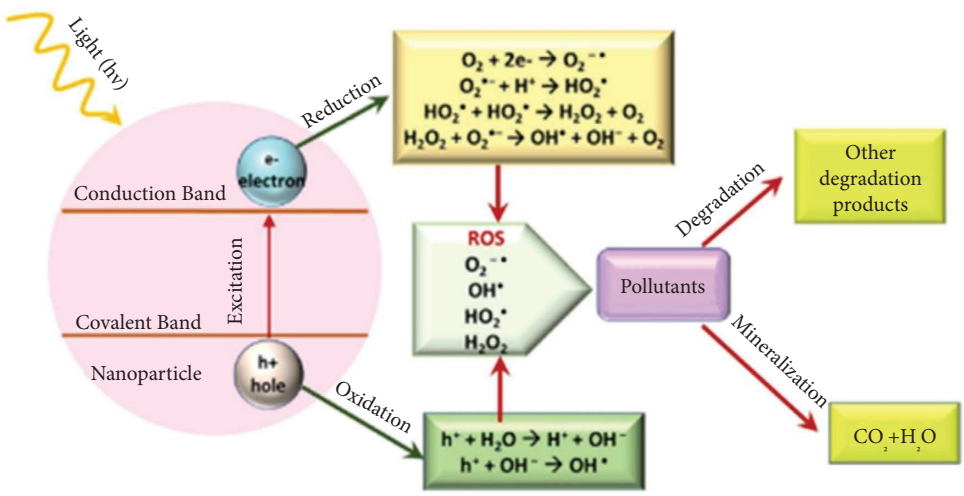

Figure 5: Photocatalysis mechanism, reproduced from reference [101] (copyright 2022, with permission from Elsevier).

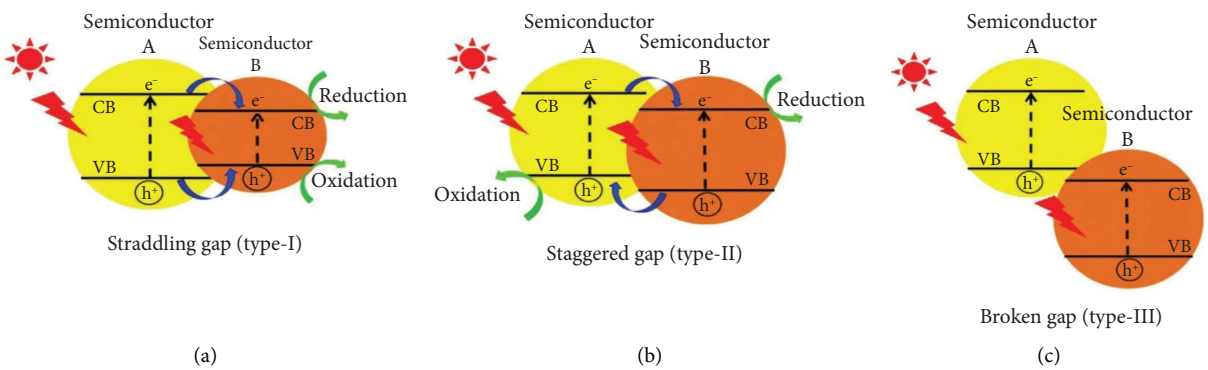

Figure 6: Types of heterojunction photocatalyst, reproduced from reference [104] (copyright 2017, with permission from Wiley).

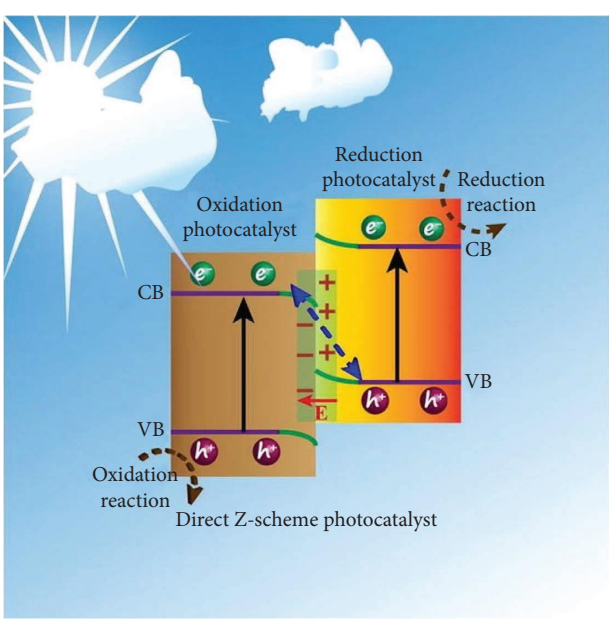

Figure 7: *Z*-scheme photocatalyst, reproduced from reference [108] (copyright 2018, with permission from Elsevier).

the AOPs, reactive species such as hydroxyl radicals (•OH) are generated that oxidize a broad range of pollutants. The combined process of solar technology and catalysis proved to be a useful process for the reduction of water pollution. Table 1 summarizes the overview of different catalysts used in the photocatalysis process. Different catalysts are used for the degradation of the dyes.

4.1. Transition Metal Oxide Catalysts. Transition metals possess multiple valency, which results in a variety of oxides and crystal structures. They are a potential catalyst due to their low toxicity and ease of preparation. Jiang et al. [109] synthesized iron oxides, namely, 2-line ferrihydrite, α-Fe_2O_3, γ-Fe_2O_3, and Fe_3O_4 by the sol-gel method. The researcher reported the orange II degradation in the presence of visible light and H_2O_2 at neutral pH. Spherical γ-Fe_2O_3 was synthesized by Liang et al. [110] for the photocatalytic removal of orange I of 20 mg/L concentration. Around 48.89% degradation and 36.5% mineralization were achieved within 6 h of visible-light irradiation. Iron oxide nanoparticles of size less than 100 nm were biosynthesized for the decolorization of orange S. Under optimal

Table 1: An overview of photocatalytic degradation of azo dyes using different photocatalysts.

Photocatalyst	Synthesis method	Pollutant	Pollutant conc	Catalyst dosage	Light	Time (min)	Kinetic (min^{-1})/ degradation (%)	Ref
Mesoporous iron oxides	Sol-gel	Orange II	0.1 mM	0.25 g/L	Visible	180	0.02	110
Magnetite (γ-Fe_2O_3)	One-step aqueous method	Orange I	20 mg/L	0.4 g/L	UV and visible	18	48.89	111
Iron oxide	Biosynthesis	Direct orange S	10 mg/L	1 g/L	Ultrasonication	60	89	112
Iron oxide	Aqueous solution process	MO	—	—	UV light	105	80	113
Fe_2O_3	Green synthesis	BB 41 AB 58	50 mg/L	0.4 g	Visible	120	77.3 82.5	114
α-Fe_2O_3	Hydrothermal	Acid redG	50 mg/L	0.1 g	LED lamp	90	98	115
Fe_2O_3	Biosynthesis	MO	10 ppm	50 mg	UV lamp	90	93.5	116
α-Fe_2O_3	Coprecipitation	MO MR	10 ppm	100 mg	UV lamp	5	94 76	117
Fe_2O_3	Combustion	MO	20 mg/L	0.05 mg	UV	100	95.3	118
TiO_2	Sol-gel route	MO	20 ppm	12 mg	Sunlight	120	79	119
TiO_2	Solvothermal	MO	0.06 M	0.3 g	Mercury Sunlight	50 40	96 94	121
TiO_2	Sol-gel route	MO	20 mg/L	4000 mg	UV Visible	180	82 72	124
TiO_2	Sol-gel	Novacron red C-2BL	—	—	UV irradiation	100	98	126
CuO	Combustion	Trypan blue	5 μg/L	100 mg	UV sunlight	150	90	127
CuO	Thermal process	MO	1×10^{-5} M	—	UV lamp	240	—	128
CuO	Precipitation	MO	20 mg/L	—	Visible	120	87	129
NiO	Coprecipitation	CR	20 ppm	5 mg	Sunlight	160	80	133
NiO	Coprecipitation	MO	30 mg/L	74 mg	UV light	210	82	134
NiO	Hydrothermal route	CR	10 mg/L	0.1 g	Visible light	30	98	135
NiO	Green synthesis	CR	10 mg/L	0.1 g	Sunlight	35	95	136
ZnO	Sol-gel	MO CR DB 38	30 mg/L	10 mg	UV lamp	25	99.45 99.70 99.21	137
ZnO	Commercially available	Acid brown 14	5×10^{-4} mol·l^{-1}	2.5 g/l	Sunlight	120	84.72	138
ZnO	Green synthesis approach	Orange 16	0.4 g in 100 mL	0.1 g	Sunlight	180	93	139
ZnO	Precipitation	EBT	20 μg/mL	10 mg	Visible UV-fluorescent	30	46.89 99.83	140
ZnO	Sol-gel	AR183	10 ppm	2 gm/L	UV light	800	79%	143
Cobalt titanate	Coprecipitation method	AR 27 AY17 AB120	50 mg L^{-1}	20 mg	—	30	100 100 80	144
$SrSnO_3$ perovskite	Pechini method	RNL	10 mg/L	60 mg	9 W UVC lamp	600	98	145
$CeNiO_3$ (CNO)	Hydrothermal	OG	2×10^{-5} mol·L^{-1}	0.2 g/L	UV light	240	95	146
Perovskite $SrTiO_3$-δ (STO)	Nitrate route	CR	10 mg/L	0.8 g/L	UV light Solar light		62 97	147

Table 1: Continued.

Photocatalyst	Synthesis method	Pollutant	Pollutant conc	Catalyst dosage	Light	Time (min)	Kinetic (min^{-1})/ degradation (%)	Ref
Lanthanum nickelate, $LaNiO_3$ (LNO)	Ultrasonication process	OG dye	3.5×10^{-5} mol/L	27 mg	Tungsten halogen lamp	24	96	148
$LaNiO_3$ perovskite	Sol-gel citrate method	RB 5	100 mg/L	1 g/L	—	—	65.4	149
$NiFe_2O_4$ nanoparticles	Green route	CR	5 mg L^{-1}	5 mg	Sunlight	75	85	150
Manganese ferrite	Chemical precipitation	RR198	100 mg/L	0.20 g	UV–C lamp	90	99 95	151
$BiFeO_3$ (BFO)	Sol-gel	Mordant blue 9	(50 mg/l)	0.1 g	Visible	180	88.5	152
Mg1-xZnxFe_2O_4	Combustion method	Reactive Blue-19	25 mg/L	20 mg	300 W Xe lamp	90	99.5	153
Zinc ferrite	Reduction-oxidation method	Orange II	100 mg/L	—	Visible	30	69.1	154
Manganese ferrite	Precipitation	CR	50 mg/L	50 mg	Xenon	30	98.3	155
α-Fe_2O_3, $NiFe_2O_4$, $ZnFe_2O_4$	Sol-gel	Amido black 10b	25 mg/L	0.1 g	Visible light	90	89 85 92	156
BiOCl	Solvothermal	MO	20 mg/L	0.3 g	UV light simulated sunlight light	20	99	157
BiOI	Template free route	MO	10 mg/L	0.20 g	Visible light	30	90.8	158
BiOBr	Solvothermal	MO	10 mg/L	0.080 g	Solar light	60	97	159
BiOI	Solvothermal	EBT MO	15 mg/L	400 mg/L	LED	60	86.7 47.4	160
BiOCl	Solvothermal method	RO84	20 mg/L	0.3 g	UV lamp sunlight	60	40 99	162
β-Fe_2O_3/g-C_3N_4	In situ growth strategy	MO	10 mg/L	1.25 g/L	Simulated solar light	240	0.43	163
Fe_3O_4@SiO_2@Rucore-shell	Three-step method	MO MR	30 mg/L	10 mg	Visible	150	0.0428 0.0338	164
ZnS/$ZnCr_2O_4$	Precipitation process	MO	40 ppm	40 mg	Visible	105	96.88	165
WO_3/SBA-15	In situ and wet impregnation	MO	100 mg/L	0.3 g/L	Visible	30	98	166
Iron oxide magnetic	Thermal decomposition process	AB10B	0.01 mM	200 mg/L	RPR3500 lamps	120	76	167
Tin-doped $BiFeO_3$/graphene	Coprecipitation method	CR	100 mg/L	—	Xenon lamp	60	100	168
Poly(azomethine)/TiO_2	Two-step synthesis	Bismarck brown	50 ppm	500 mg	Sunlight	300	95	169
CdS/Ag	Coprecipitation	RR 120	50 ppm	50 mg	UV solar light	120 75	93 93	170
		AB 1	10 ppm	10 mg	UV solar light	50 30	95 92	
		DB 15	10 ppm	10 mg	UV solar light	50 35	94 92	
F-SCN	Thermal polymerization	MO	10 mg/L	50 mg	Visible light	60 min	77%	171
CS-BiOCl/ZnO	Hydrothermal route	CR	1 mg/100 mL	50 mg	UV light	40	93	172
rGO-Poly[ViEtIm]-[PW12O40]	Anion exchange	MO	50 mg/L	20 mg	—	180	98.7	173
Pt–Au/TiO_2/$BaFe_{12}O_1$	Electrospun	AR 14	0.05 mg/L	50 mg	Tungsten light	120	95.2	174
Ag_2O/$CuWO_4$	Coprecipitation method	AO 7	15 mg/L	(1 g/L)	Sonocatalytic	60	84.7	175

Table 1: Continued.

Photocatalyst	Synthesis method	Pollutant	Pollutant conc	Catalyst dosage	Light	Time (min)	Kinetic (min^{-1})/ degradation (%)	Ref
CoZnO/PVA	Coprecipitation method	MO	—	—	UV-vis light radiation	48	98	176
$ZnAlxB_2$–xO_4	Solution combustion method	RB 5	10^{-5} M	0.1 g	Sunlight	60	98	178
NiO/TiO_2	Chemical reduction method	Orange II	50 ppm	0.02 g	UV light	30	96	179
F, Sm^{3+} codoped TiO_2/MWCNTs	Sol-gel	Brilliant black BN	50 mg/L	100 mg	Visible light region	180	99	180
MWCNTs/$CoFe_2O_4$	Coprecipitation	AB113	25 mg/L	0.4 g/L	UV light	60	100	181
TiO_2@Cd-MOF)	Sol-gel method	MO	10 mg/L	10 mg	Visible-light	60	94.1	182
TiO_2@Fe_3O_4@C-NFs	Hydrothermal	Azo dye	—	100 mg	UV-halogen-lamp	200	90	183
ZnO nanorods	Seed-mediated	AR 88	20 mg/L	—	UV light A	180	97	184
(Ce0.92Cu0.04Bi0.04O2)	Hydrothermal	MO	10 mg/L	10 mg	Solar light	50	95.79	185
CeO_2/ZrO_2	Coprecipitation method	Orange G	10 ppm	0.20 g/L	Solar light	400	90	186
FeOxrGO/Ti	Wet impregnation	RB5	10 mg/L	—	Solar light	120	99.9	187
Bimetallic FeNi alloy	Precipitation	CR	250 mg/L	80 mg	—	150	99.41	188
$MnFe_2O_4/\alpha$-MnO_2	Hydrothermal	Orange G	2.5 mL	0.5 mL	—	30	96.8	189
BiOCl-Cu_2CoSnS_4-TiO_2	Coprecipitation method	DB 71	20 mg/L	100 mg	Sunlight	60	91.4	190
Ag/Ag_3PO_4-BiOBr-C_3N_4	Coprecipitation method	RR120	20 ppm	100 mg	Sunlight	30	92.6	191

conditions, 87.2% of the dye was removed at pH 9 by Karthikeyeni and his coworkers [111]. Sharma et al. [112] reported (α-Fe_2O_3) nanocubes synthesized by a low-temperature aqueous solution process for efficient degradation of MO with 80% efficiency under UV light. Ali et al. [113], in this study, prepared α-Fe_2O_3 from the mandarin peels and showed the photodegradation of basic maxilon blue GRL 300% and acidic neolan blue 2G. Burger shape morphology of α-Fe2O3 catalyst reported by Xiao et al. [114] synthesized by the facile hydrothermal method. The catalyst exhibited 98% degradation efficiency and 62% COD removal rate for acid redG in aqueous solution. Weldegebrieal et al. [115] synthesized Fe_2O_3 using *V. amygdalina* leaves extract. The degradation of MB and MO dyes was investigated under sunlight irradiation. Gupta et al. [116] reported coral-shaped Fe_2O_3. The photocatalyst showed a fast degradation efficiency of around 94% within 5 min in UV/H_2O_2 in a 32 W system for azo dye MO. Recently, α-Fe_2O_3 nanoparticles were synthesized by the combustion process of organic fuels. The degradation efficiency under UV radiation obtained for MO degradation is 95.31% which was synthesized using sucrose [117].

Sheikh et al. [118] synthesized TiO_2 at low temperature via a greener sol-gel approach. The researcher reported the photocatalytic potentiality for the photodegradation of azo dyes, MO, and CR. The effect of thermal treatment on photocatalytic activity and morphology of TiO_2 was reported by Allen et al. [119]. Raju and Kale [120] designed flower-like rutile TiO_2 using the solvothermal method. The photocatalyst under mercury and sunlight showed 96 and 94% degradation within 50 and 40 min, respectively. Dave and Chauhan [121] synthesized TiO_2 for the dye degradation of DB 14 under visible light. Around 99% of the dye degraded after 10 min. TiO_2 nanofibres were reported by Secundino-Sánchez et al. [122] and they evaluated the photocatalytic activity by decoloration of Remazol Black B azo dye. Saensook and Sirisuk [123] synthesized black TiO_2 by a chemical reduction for MO dye degradation under both UV and visible-light irradiations. The researcher found 82.17% efficiency under UV light. Vacca et al. [124] performed the optimization of MO dye removal with TiO_2 nanotubes. Redha et al. [125] prepared TiO_2 nanofilms by the sol-gel method, and a reactor was fabricated. The degradation of novacron red c-2BL (98%) was achieved within 100 min under UV light.

Copper oxide nanoparticles were synthesized by Lingaraju et al. [126] using the solution-combustion method using green fuel *Rauvolfia serpentina*. The photodegradation performance was evaluated by degrading trypan blue dye. Scuderi et al. [127] reported the catalytic efficiency of synthesized CuO and Cu_2O nanowires by evaluating MO degradation by a UV lamp. Novikova et al. [128] prepared CuO nanostructures by the precipitation method for the investigation of the photocatalytic activity of MO. CuO nanoparticles were synthesized using *Spirulina platensis*. The CR dye degradation was evaluated by Alsamhary et al. [129]. Aroob et al. [130] reported CuO nanoparticles by a mechanochemical approach using a green reducing agent *Seriphidium oliverianum*. The degradation rate obtained for MO is 65.078%. Cu_2O catalyst was evaluated for decolorization of RR180 and BR18 dye by Polat et al. [131]. The removal efficiency for RR180 and BR18 was observed to be 100% and 94.34%.

Bhat et al. [132] synthesized FCC-structured NiO by the coprecipitation method. The concentration of the initial dye on photocatalytic effect was evaluated by degrading CR dye. Sabouri et al. [133] synthesized NiO nanosheets by the coprecipitation method, and degradation of MO is reported. Around 82% of MO degradation was achieved within 210 min. Hydrothermal route was adopted for the preparation of NiO nanocubes by Sun et al. [134]. The degradation efficiency for CR was achieved within 30 min of irradiation. Roopan et al. [135] prepared NiO particles using the capping agent *Calotropis gigantea* latex. Under sunlight irradiation, 95% of CR degradation was observed.

Chen at al. [136] reported a sol-gel method for ZnO photocatalyst, and 99.70% removal of MO was observed under UV radiation. Sakthivel et al. [137] compared and investigated acid brown 14 degradation under solar light with commercially available TiO_2. The decolorization was achieved within 120 min of irradiation. Al-Zahrani et al. [138] created ZnO-NPs using leaf extract of *P. granatum* for photocatalytic degradation of orange 16 dye. Lanjwani et al. [139] synthesized ZnO by complexation reaction between zinc acetate and sodium diethyldithiocarbamate trihydrate. The photocatalytic efficiency was evaluated for EBT dye under UV, visible, and mercury light irradiation. Meanwhile, the ZnO nanosphere catalyst is synthesized by hydrothermal route for MO dye under UV radiation [140]. Sansenya et al. [141] prepared ZnO by a hydrothermal method for the complete photodegradation of RR141 and CR dye. ZnO nanoswirlings fabricated by Umar et al. [142] observed 79% AR183 dye degradation under UV light within 80 min.

4.1.1. Perovskite-Type Oxides. The general formula of perovskite is ABO_3 where cation A is of larger size and belongs to perovskite-type oxides. These materials have drawn outstanding interest towards energy conversion and environmental remediation due to their unique optical, physiochemical, electrical, structural, and thermal properties. Lin et al. [143] synthesized perovskite cobalt titanate and employed it for the degradation of AR 27, AB 120, and AY 17 azoic dyes. Perovskite $SrSnO_3$ photocatalyst is synthesized by Teixeira and his coworkers [144]. The degradation of Remazol golden yellow was observed under UV radiation with 98% efficiency. $CeNiO_3$ was synthesized by hydrothermal approach by Maridevaru et al. [145] and assessed the photocatalyst under UV irradiation for the removal of orange G. Merrad et al. [146] reported the synthesis of deficient perovskite $SrTiO_{3-\delta}$ and photooxidation of CR under both UV light and solar irradiation, respectively. Maridevaru et al. [147] synthesized nanocubes of $LaNiO_3$ and examined visible degradation with 96% rate for orange G azo dye. The catalytic wet air oxidation process was investigated by Palas et al. [148] for the removal of RB 5 of 100 mg/L concentration.

4.2. Spinel Metal Ferrites. A spinel ferrite crystal possesses a unit formula of AFe_2O_4. These are formed by the combination of a trivalent cation and another divalent metallic cation, and they have a face-centered cubic core. The cations are arranged according to the different crystallographic sites, i.e., tetrahedral sites and octahedral crystallographic sites surrounding oxygen atoms.

$NiFe_2O_4$ NPs were synthesized by Taj et al. [149], and photocatalytic degradation of CR was achieved with 85% of removal. Manganese ferrite nanoparticle (MFN) was prepared by Mahoodi [150] for the degradation of RR198 and RR 120 azo dye as model compounds. Ćirković et al. [151] reported a single-phase $BiFeO_3$ultrasound-assisted sol-gel route for Mordant blue 9 degradation. The synthesis of $Mg_{0.5}Ni_xZn_{0.5\text{-}x}Fe_2O_4$ was reported by Dhiman et al. [152], and within 90 min, visible-light degradation can be achieved with 99.5% efficiency. $ZnFe_2O_4$ photocatalyst was fabricated by Cai et al. [153] for catalytic degradation of orange II decolorization under 150 W visible light. Ramadoss et al. [154] synthesized $MnFe_2O_4$ and revealed 98.3% CR dye in a photocatalytic reactor within 30 min. El-Salamony et al. [155] reported photodegradation of Amido black b10 dye using $ZnFe_2O_4$ with 92% degradation efficiency.

4.3. Bismuth Oxyhalide. An emerging class of materials, bismuth oxyhalide (BiOX), exhibits excellent photocatalytic properties due to its exceptional layered and attractive band structure. BiOX materials were earlier used for storage and as ferroelectric materials. However, recently, its wide applications have been explored in various fields, especially in the purification of wastewater.

Sun et al. synthesized BiOCl via a solvothermal process using methanol as solvent, and degradation of MO is reported under sunlight [156]. Flower-like BiOI was prepared by Wang et al. [157] for MO degradation under the visible-light irradiation. BiOBr was reported by Mera et al. [158] for MO dye, with 97% degradation within 60 min under simulated solar radiation. Nourzad et al. [159] synthesized BiOI by solvothermal technique and evaluated degradation of MO and EBT with a removal efficiency of 47.4% and 86.7%, respectively, using an LED light. Yu and Han [160] prepared BiOX (X = Cl, Br), and MO degradation is investigated. BiOCl microspheres were synthesized by Mendez-Alvarado and his coworkers [161] by the solvothermal method for catalytic degradation of RO84 under sunlight.

4.4. Hybrid Nanomaterial. Among these, semiconductor/semiconductor-based photocatalysts instead of single semiconductors are more efficient and practical approaches to enhance photocatalytic performance. Due to the coupling and synergistic effects resulting from heterogeneous interfaces, the system not only possesses the corresponding physicochemical properties of its individual component but also exhibits superior or completely new characteristics. Christoforidis et al. [162] prepared hybrid β-Fe_2O_3/g-C_3N_4 nanomaterial *via* a facile in situ growth strategy embedded in a solid state process. Their photocatalytic activity was evaluated under both simulated solar light and pure visible-light irradiation against the photodegradation of MO dye. The β-Fe_2O_3 content in the final material was tuned to optimize the photocatalytic performance, with particular attention to the activity under visible light. Kumar et al. [163] synthesized a hybrid Fe_3O_4@SiO_2@Ru composite for the removal of MR and MO under irradiation of visible light. The composite showing better stability and repeating cycles greater than 90% was obtained. Palanisamy et al. [164] fabricated $ZnS/ZnCr_2O_4$ by the simple precipitation method. The amino acid (methionine) is used as a capping agent and showed enhanced photodegradation MO with four repeating cycles. A heterogeneous catalyst, Au-WO_3/SBA-15 catalyst, fabricated by Malik et al. [165] efficiently degraded high concentration of MO dye at a pH 2 value pollutants ($C = 0.3\ g{\cdot}l^{-=}$) within 30 min and can retain a good degradation efficiency at a pH value of 2. Aiello et al. [166] synthesized MNC-PMAO-PN nanohybrids and performed the photodegradation experiments for acid black 10B azo dye. Around 76% degradation efficiency is observed without the addition of an external oxidising agent. Tin-doped bismuth ferrite nanoparticles-graphene nanoplatelets (BFSO/GNP) were prepared by Fatima and Rizwan [167]. The efficient dye removal is observed with 10 cycles of catalytic activities. Pradeeba et al. [168] degraded azo dye, cationic azo dye, and Bismarck brown by poly (azomethine)/TiO_2 photocatalyst. Ravikumar et al. [169] reported a CdS/Ag photocatalyst for efficient degradation of RR120, AB 1, and DB 15 azo dyes under UV and solar light irradiation. The studies demonstrated 93% of degradation within 75 min and a high repeatability cycle. A doped carbon nitride photocatalyst was prepared by Yang et al. [170]. The doping of F and S elements with (g-C_3N_4) enhanced the degradation rate of MO dye. Ranjithkumar et al. [171] by modified hydrothermal route fabricated CS-BiOCl/ZnO nanocomposite for the photodegradation of Congo red. The catalyst degraded 93% dye under UV light within 40 min. Zhang et al. [172] demonstrated rGO-poly[ViEtIm]Br as a platform to degrade MO dye. The degradation efficiency is 98.7% in 3 hours. Razavi et al. [173] synthesized Pt–Au/TiO_2/$BaFe_{12}O_{19}$ nanofibres and investigated for AR 14 dye with 95.2%, with the reaction rate coefficient of 0.0247 min^{-c}. The $Ag_2O/CuWO_4$ composite demonstrated effective degradation of acid orange 7 [174]. Codoped ZnO-NPs were synthesized by using polyvinyl alcohol hydrogel for MO dye degradation. The CoZnO/PVA composite showed photocatalytic efficiency and completely mineralized MO in 48 min [175]. Kang et al. [176] synthesized Fe_3O_4 @Al-MOF for the removal of CR with 83.7% upto five cycles. Cubic mesoporous $ZnAl_xB_{2-x}O_4$ were synthesized and calcined at 700°C for 3 h by the solution-combustion method by Mukherjee and his coworkers [177] and they evaluated for the degradation of reactive black 5 dye. NiO/TiO_2 composite was prepared by Gul et al. [178] for the degradation of orange II dye with 96% degradation within 30 min. Mukonza et al. [179] adopted the sol-gel technique and reported Fluorine-Sm^{3+} codoped TiO_2 (0.6% Sm^{3+}) catalyst for the degradation of

brilliant black BN bisazo dye within 3 hours of simulated solar irradiation. The total organic carbon removal was 82%. The researcher demonstrated that F and Sm^3 incorporation improved the optical properties, surface chemistry, and quantum efficiency properties. Further reaction kinetics increased, and reaction time was improved by the incorporation of MWCNTs. Meanwhile, Al-Musawi et al. [180] completely degraded AB113 dye at pH = 3 using MWCNTs/$CoFe_2O_4$ by the sonophotocatalytic process within 40 min. The optimum parameters for 100% AB113 removal with catalytic dose is 0.4 g/L, at pH 3. The UV light of 36 W was used as a light source. Highly porous three-dimensional TiO_2@Cd-MOF was fabricated by Ramasubbu et al. [181] by sol-gel technique and they further prepared TiO_2@Cd-MOF)@ZnPp and evaluated for MO degradation. Around 94.1% degradation efficiency was achieved with good recycle tests. The researcher revealed that optical absorption and efficient electron injection further improved the photocatalytic activity. A multifunctional TiO_2@Fe_3O_4@C–NF hybrid material is reported by Yilmaz et al. [182] for azo dye degradation. The degradation efficiencies reached 80–100% within 8–125 min under UV irradiation. The prepared sample showed high repeatability, efficiency, and sustainability. Kardeş et al. [183] fabricated flexible photocatalyst 3D polyurethane (PU) foam struts aligned with ZnO nanorods. The hybrid photocatalyst structural integrities analysis showed that ZnO layers remained intact and adherent on the surfaces even after 1 h of sonication. Azo dye, AR 88, was tested in a laboratory-scale photoreactor for color removal efficiency and total organic carbon content. The efficiency obtained is 97% within 180 min under UVA light. The hydrothermal method is adopted by Ishfaq et al. [184] for synthesizing doped CeO_2 ($Ce_{0.92}Cu_{0.04}Bi_{0.04}O_2$). The researcher demonstrated that doping copper and bismuth improved the current conductivity and light harvesting synergistically. Under solar irradiation, the catalyst degraded 95.79% MO dye within 50 min at the rate of 0.0314 min^{-t}. The dye mineralization is also five times faster than a CeO_2 photocatalyst with robust reusability tests. Orange G photodegradation was evaluated by chitosan-modified CeO_2/ZrO_2 under solar light by Nisha et al. [185]. The synthesized catalyst obtained band gap energy of 2.9 eV with an average crystalline size of 30 nm. Zhang and Shih [186] reported FeO_xrGO/Ti photoanodes and photoelectrocatalytic degradation of azo dye. The incorporated rGO enhanced the electrochemical surface area of the anode which substantially improved the catalytic property. FeNi@GR nanoparticles prepared by Zou et al. [187] demonstrate that the synergistic effect between bimetals and the electron transfer ability of graphene within 150 min efficiently removed CR dye. Thao et al. [188] evaluated the orange G degradation by $MnFe_2O_4$/α-MnO_2 in peroxymonosulfate activation. Around 96.8% of orange G degradation was achieved within 30 min regardless of solution pH changes. Chowdhury et al. [189] synthesized ternary BiOCl-Cu_2CoSnS_4-TiO_2 nanocomposite and evaluated the degradation of direct blue 71 azo dye. Gogoi et al. [190] fabricated quaternary Ag/Ag_3PO_4-BiOBr-C_3N_4 composite for anionic pollutant RR 120 dye.

5. Photocatalyst Surface Charge Interaction with Dyes

The surface charge of a photocatalyst (zeta potential) and dye interaction is considered as a vital factor for enhancing the photocatalytic activity. The redox reaction and charge carrier movements occur at the photocatalyst surface. Thus, improvement in surface modification can pave an effective photocatalytic activity. The surface charge (zeta potential) of the catalyst is influenced by the pH of the medium. Borthakur et al. [191] reported the Ag/rGO nanocomposite for the CR anionic diazo dye degradation. The zeta potential of Ag/rGO nanocomposite materials was analyzed by the following equation:

$$\zeta = \frac{4\pi\eta}{\mathrm{Dt}} \times \mu, \tag{1}$$

where ζ denotes the zeta potential, μ signifies the electrophoretic mobility, η is the viscosity, and Dt is the dielectric constant of the medium. The experiments were conducted in the pH range from 2 to 11. It was found that the Ag/rGO nanocomposite surface is negatively charged. As the pH medium increases, the surface charge of the nanocomposite becomes more negative. This is due to the functional group present on the graphene sheets. Conversely, with a decrease in the acidic medium, the surface becomes positive. The CR dye is an anionic molecule. Therefore, in an acidic medium, the interaction of the dye is high, and a maximum degradation of 95.55% is observed at pH 3. Meanwhile, another study by Mittal and Khanuja [192] for the $MoSe_2$-PANI composite found that the highest photocatalytic degradation efficiency is obtained in MP21 due to its optimized surface charge. $MoSe_2$ zeta potential is −23.01 mV, whereas PANI is positively charged with 9.51 mV. The zeta potential of the composite MP21 sample is −5.7 mV. Thus, RhB molecules being a cationic dye would preferably adsorb on the $MoSe_2$ surface and CR molecules being an anionic dye adsorb on the PANI surface. Another work investigated by Borthakur and Das [193] reported the surface potential values of NiS_2-rGO and CoS-rGO nanocomposite and evaluated the photodegradation efficiency of CR dye. Verma et al. [194], in their experimental results, obtained that 3% Au–ZnO nanorods composite found that with an increase in alkaline medium 10, the zeta potential was found to be about 5.5 mV, while at pH 3, it is 33.1 mV. Thus, in an acidic medium, there was an increase in zeta potential. At the basic condition, hydroxylated surface deprotonation occurred, which results into decreased zeta potential, or at lower pH medium, hydroxylated surface protonation attributed to positive surface charge.

6. Factors Affecting the Degradation of Dyes

The dye degradation by a photocatalyst depends on certain parameters such as pH, photocatalyst particle concentration, initial dye concentration, and light intensity. These parameters are discussed influencing the photodegradation of dyes.

6.1. Catalyst Dosage. Generally, with the increase in catalyst amount, photodegradation increases. This is due to the availability of more active sites which can absorb more photons under irradiation and produce more OH• radicals and positive holes. However, beyond a certain limit, if catalyst dosage is increased, the photodegradation rate decreases which might be due to the formation of a turbid solution so that UV/Vis radiation is not percolated in the water. The nanoparticles agglomerate which reduces the active surface sites available for exposure results in a coagulation of catalyst particles [195, 196].

6.2. Effect of pH. The pH is an effective factor in the photocatalyst degradation of azo dyes. The pH can affect the ionization level of the photocatalyst. The pH variation impacts the photocatalyst oxidation process. The hydroxyl radicals are formed by the reaction between hydroxide ions and positive holes. Also, in the lower pH, the positive holes are vital oxidising species, whereas at neutral or higher pH, hydroxyl radicals are the dominant species [197].

6.3. Effect of Dye Concentration. The initial dye concentration in photocatalytic degradation plays an important role. On increasing dye concentration and with a fixed amount of photocatalyst, the degradation rate decreases. This might be due to the presence of more organic pollutants which are adsorbed on the surface of the photocatalyst, and so, photons are unable to get on the catalyst surface. Hence, there is less active species formed and so a decrease in decolorization percentage [198, 199].

6.4. Effect of Irradiation Time and Intensity of Light. The light intensity, source, and irradiation time greatly influence the photodegradation of pollutants. In general, a photocatalyst absorbs light energy equal to or more than the band gap energy. This further causes the electrons to transfer from VB to CB leaving behind holes in the VB. Thus, when the intensity of incident light is high, the excitation of the photocatalyst is also high, and thus, the photodegradation rate can be enhanced [200, 201]. Natural sunlight is a cost-effective light source. However, nowadays, artificial UV and solar simulators are more reproducible. Ollis et al. [202] investigated that the rate of degradation occurs linearly (first order) on increasing the light intensity. At intermediate, the light intensity rate would depend on the square root of the light intensity (half order). Hence, by increasing the number of photons, the probability of activation of photons on the surface of the catalyst enhances.

7. Role of Active Species in Photodegradation of Dye

Photocatalytic degradation is the light-driven process for pollutant degradation. A redox reaction occurs by the photocatalyst upon interaction with the dye molecule in the presence of light. The photon absorption in the first step leads to the formation of photogenerated electron and hole pairs [203]. These electron/hole pairs generated further react with oxygen, water, and hydroxyl groups and form reactive oxygen species such as hydroxyl (•OH) and superoxide ($•O_2^-$) radicals and hydrogen peroxide (H_2O_2). To determine the active species responsible for the photocatalytic experiment, different scavengers are added to trap and remove active species [204]. The hydrogen peroxide is a stable molecule compared to the superoxide radical. The hydroxyl radicals (•OH) are usually trapped by adding isopropanol (IPr), ethanol (EtOH), and methanol (MeOH). [205, 206]. For superoxide anion radical ($•O_2^-$), the scavengers used are p-benzoquinone (p-BQ) and ascorbic acid (AA) [207–209]. The scavengers such as ethylenediaminetetraacetic acid (EDTA), triethanolamine (TEA), sodium oxalate ($Na_2C_2O_4$), and sodium iodide (NaI) are usually used to scavenge holes [210–212]. For the electrons, the scavengers used are potassium bromate ($KBrO_3$), potassium persulfate ($K_2S_2O_8$), and ammonium persulfate $(NH_4)_2S_2O_8$) [212–214]. The singlet oxygen ($^1O_2$) is determined by adding sodium azide (NaN_3) [215]. Christoforidis et al. [162] investigated the active species role by control experiments on the FCN-3 sample. For the reaction, tert-butyl alcohol (TBA) was used as hydroxyl radical (OH•) and triethanolamine (TEOA) for hole (h^+) scavenging. The superoxide radicals (O_2−•) were analyzed by control experiments under a saturated argon atmosphere. The photogenerated h^+ is the dominant species responsible for the degradation of MO, as the degradation process was greatly suppressed in the case of the FCN-3 sample. Palanisamy [164] in their study confirmed the reactive species role by using isopropanol for OH• radical, benzoquinone for (O_2−•), and triethanolamine for h^+ radical. The researcher observed that with the addition of BQ and IPA scavenger, degradation efficiency decreased to 60.1 and 24.2% from 98.66%, respectively. This indicates that the holes did not take part in the photodegradation process and OH• and O_2−• species initiated the breaking of MO dye molecules. Kardeş and his group evaluated the scavenger experiments for AR88 dye solutions by conducting the experiments under UVA light for 240 min. Here, propanol, formic acid, and l-ascorbic acid were used as trapping agents for •OH, h^+, and $·O_2$, radicals, respectively. Figure 8 illustrates the degradation efficiencies for the dye ZnO/PU samples in the presence of scavengers [183].

It was observed that the degradation efficiency (83.5%) is slightly suppressed in the presence of formic acid and 2-propanol (63.2%) indicating that OH and h+ radicals have little effect on degradation process. The efficiency intensely decreased from 95.3 to 58.1% after the addition of l-ascorbic acid. The results indicated that O_2^- radicals are markedly inhibited by l-ascorbic acid.

Another researcher group investigated reactive species formed in the degradation process by trapping experiments for AB113 dye in the presence of isopropanol (IPA), ethylenediaminetetraacetic acid (EDTA), and benzoquinone (BQ) for •OH, h+, and $•O_2^-$, radicals, respectively. The results showed that 100% efficiency is obtained in the absence of any scavenger. In addition to IPA and EDTA, removal efficiencies decrease by 42% and 35% indicating that

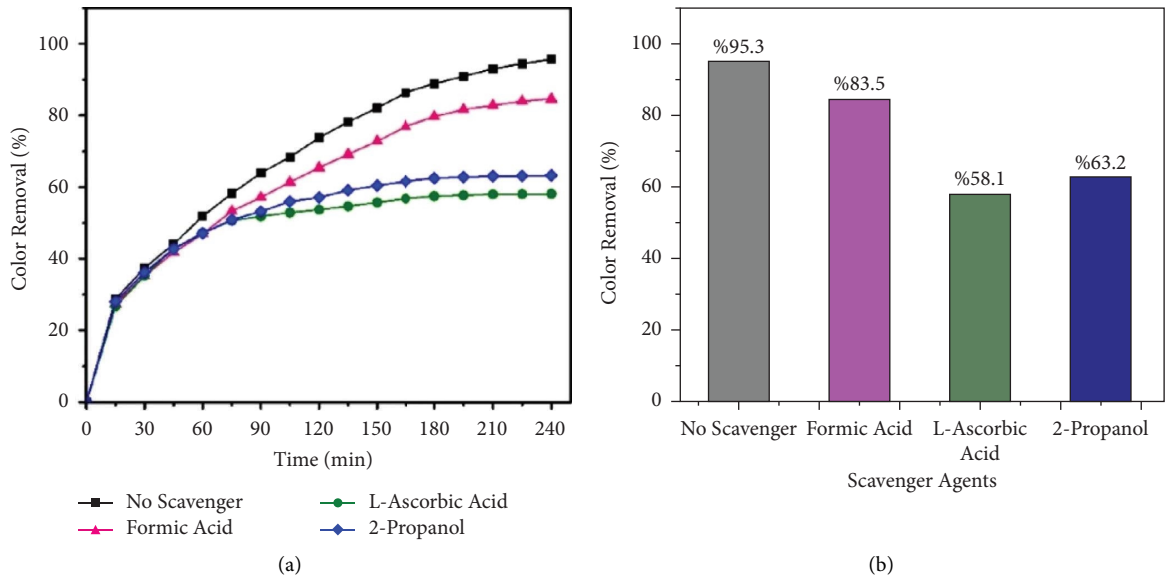

Figure 8: (a) Percentage color removal efficiencies of the AR88 dye solutions for ZnO/PU nanohybrid samples and (b) percentage color removal as a function of scavengers, reproduced from reference [178] (copyright 2023, with permission from ACS).

•OH and h^+ are solely responsible for the degradation process [180]. Thao et al. [188] showed that after the addition of TBA, FFA, p-BQ, and EtOH in the orange G dye solution with $MnFe_2O_4/\alpha\text{-}MnO_2$/PMS catalyst, degradation efficiency decreased to a great extent compared to without adding scavenger 96.8%. The order of active radicals formed in the system is SO_4 •− > O_2 •− > $1O_2$ > HO•. Furthermore, DMPO and TEMP analyses were used to detect radicals. Also, the EPR results confirmed the active role of SO_4 •−, O_2 •−, and $1O_2$, in catalytic reaction.

8. Conclusion and Future Prospects

Dye effluent's presence causes water pollution and is a major concern for the environment. Till date, efficient dye removal techniques have been explored. In this review, we concluded various dye removal techniques such as biological, chemical, and physical methods. The idea was to make readers informed of the existence along with modern methods available for removing organic pollutants from wastewater. The aim of this paper is to highlight an advanced nano-photocatalysis process that is recognized as an effective method for removing dye completely from waste water. In this review, the basic theory of photocatalysis and its mechanism is discussed. The photocatalysis technique is simple, powerful, and a promising technology for dye remediation, and the photocatalysts used have several advantages such as nontoxic, stable, and reusable and have a high effective activity. Further various parameters affecting degradation rate and active radical species generated in the photocatalytic process are highlighted.

Forthcoming studies can be focussed and addressed on the following:

(1) Despite modern strategies adopted, still photocatalyst suffer from problems such as extended visible-light absorption, efficiency, and prolonged lifespan
(2) The photocatalyst reusability and large scale remain a significant challenge
(3) The researcher should perform experiments with real industrial dye effluents
(4) There is a lack of sufficient information on the spent catalyst disposal
(5) The structure-activity, reactions pathway, and photocatalytic mechanism still needs depth examination with advanced characteristic technology and supported theoretical calculations

Notations

VB: Valence band
CB: Conduction band
UV: Ultraviolet
Ppm: Parts per million
COD: Chemical oxygen demand
TOC: Total organic carbon
ADMI: Dye Manufacturers' Institute
APM: Ammonium phosphomolybdate
PANI: Polyaniline
F-SCN: Sulfur fluoride-doped carbon nitride
RB 5: Reactive black 5
MO: Methyl orange
MB: Methylene blue
EBT: Eriochrome Black T
EY: Eosin yellow
MG: Malachite green
MR: Methyl red
AR: Acid red
DR: Direct red

DB: Direct blue
BR: Brilliant red
RR: Reactive red
AR: Acid red
AB: Acid blue
RO: Reactive orange
OG: Orange G
RNL: Remazol golden yellow
AB10B: Amido black 10b.

Data Availability

The data supporting this review are available from previously reported studies and datasets, which have been cited.

Conflicts of Interest

The authors declare that they have no conflicts of interest.

Authors' Contributions

Arpita Paul Chowdhury wrote the original manuscript and reviewed the draft, K. S. Anantharaju and K. Keshavamurthy reviewed the manuscript, and Samuel Lalthazuala Rokhum supervised the manuscript.

References

[1] N. Y. Donkadokula, A. K. Kola, I. Naz, and D. Saroj, "A review on advanced physico-chemical and biological textile dye wastewater treatment techniques," *Reviews in Environmental Science and Biotechnology*, vol. 19, no. 3, pp. 543–560, 2020.

[2] R. L. Singh, P. K. Singh, and R. P. Singh, "Enzymatic decolorization and degradation of azo dyes– a review," *International Biodeterioration & Biodegradation*, vol. 104, pp. 21–31, 2015.

[3] F. Amalina, A. S. A. Razak, S. Krishnan, A. W. Zularisam, and M. Nasrullah, "Dyes removal from textile wastewater by agricultural waste as an absorbent– a review," *Cleaner Waste Systems*, vol. 3, Article ID 100051, 2022.

[4] E. A. Azzopardi, S.-E. Owens, M. Murison et al., "Chromophores in operative surgery: current practice and rationalized development," *Journal of Controlled Release*, vol. 249, pp. 123–130, 2017.

[5] D. Pathania, A. Araballi, F. Fernandes et al., "Cost effective porous areca nut carbon nanospheres for adsorptive removal of dyes and their binary mixtures," *Environmental Research*, vol. 224, Article ID 115521, 2023.

[6] S. Benkhaya, S. M' rabet, and A. el Harfi, "A review on classifications, recent synthesis and applications of textile dyes," *Inorganic Chemistry Communications*, vol. 115, Article ID 107891, 2020.

[7] S. H. Hashemi and M. Kaykhaii, "Azo dyes: sources, occurrence, toxicity, sampling, analysis, and their removal methods," in *Emerging Freshwater Pollutants*, pp. 267–287, Elsevier, Amsterdam, Netherlands, 2022.

[8] G. M. Didier de Vasconcelos, J. Mulinari, S. M. de Arruda Guelli Ulson de Souza, A. A. Ulson de Souza, D. de Oliveira, and C. J. de Andrade, "Biodegradation of azo dye-containing wastewater by activated sludge: a critical review," *World Journal of Microbiology and Biotechnology*, vol. 37, no. 6, p. 101, 2021.

[9] H. Karimi-Maleh, H. Beitollahi, P. Senthil Kumar et al., "Recent advances in carbon nanomaterials-based electrochemical sensors for food azo dyes detection," *Food and Chemical Toxicology*, vol. 164, Article ID 112961, 2022.

[10] J. Aguilar-Rosero, M. E. Urbina-López, B. E. Rodríguez-González, S. X. León-Villegas, I. E. Luna-Cruz, and D. L. Cárdenas-Chávez, "Development and characterization of bioadsorbents derived from different agricultural wastes for water reclamation: a review," *Applied Sciences*, vol. 12, no. 5, p. 2740, 2022.

[11] H. R. Dihom, M. M. Al-Shaibani, R. M. S. Radin Mohamed, A. A. Al-Gheethi, A. Sharma, and M. H. B. Khamidun, "Photocatalytic degradation of disperse azo dyes in textile wastewater using green zinc oxide nanoparticles synthesized in plant extract: a critical review," *Journal of Water Process Engineering*, vol. 47, Article ID 102705, 2022.

[12] Y. Deng and R. Zhao, "Advanced oxidation processes (AOPs) in wastewater treatment," *Current Pollution Reports*, vol. 1, no. 3, pp. 167–176, 2015.

[13] S. Benkhaya, S. M'rabet, and A. el Harfi, "Classifications, properties, recent synthesis and applications of azo dyes," *Heliyon*, vol. 6, no. 1, p. 3271, 2020.

[14] P. Akhter, A. Arshad, A. Saleem, and M. Hussain, "Recent development in non-metal-doped titanium dioxide photocatalysts for different dyes degradation and the study of their strategic factors: a review," *Catalysts*, vol. 12, no. 11, p. 1331, 2022.

[15] S. Sandhya, "Biodegradation of azo dyes under anaerobic condition: role of azoreductase," *The Handbook of Environmental Chemistry*, vol. 9, pp. 39–57, 2010.

[16] A. Gürses, M. Açıkyıldız, K. Güneş, and M. S. Gürses, "Classification of dye and pigments," *Dyes and Pigments*, pp. 31–45, 2016.

[17] B. Senthil Rathi and P. Senthil Kumar, "Sustainable approach on the biodegradation of azo dyes: a short review," *Current Opinion in Green and Sustainable Chemistry*, vol. 33, Article ID 100578, 2022.

[18] R. Kishor, D. Purchase, G. D. Saratale et al., "Ecotoxicological and health concerns of persistent coloring pollutants of textile industry wastewater and treatment approaches for environmental safety," *Journal of Environmental Chemical Engineering*, vol. 9, no. 2, Article ID 105012, 2021.

[19] L. Sun, Y. Mo, and L. Zhang, "A mini review on bioelectrochemical systems for the treatment of azo dye wastewater: state-of-the-art and future prospects," *Chemosphere*, vol. 294, Article ID 133801, 2022.

[20] Y. Shi, Z. Yang, L. Xing, X. Zhang, X. Li, and D. Zhang, "Recent advances in the biodegradation of azo dyes," *World Journal of Microbiology and Biotechnology*, vol. 37, no. 8, p. 137, 2021.

[21] I. Ihsanullah, A. Jamal, M. Ilyas, M. Zubair, G. Khan, and M. A. Atieh, "Bioremediation of dyes: current status and prospects," *Journal of Water Process Engineering*, vol. 38, Article ID 101680, 2020.

[22] H. Gomaa, M. Y. Emran, and M. A. El-Gammal, "Biodegradation of azo dye pollutants using microorganisms," in *Handbook of Biodegradable Materials*, pp. 1–29, Springer International Publishing, New York, NY, USA, 2022.

[23] S. S. Ali, R. Al-Tohamy, and J. Sun, "Performance of Meyerozyma caribbica as a novel manganese peroxidase-producing yeast inhabiting wood-feeding termite gut

symbionts for azo dye decolorization and detoxification," *Science of the Total Environment*, vol. 806, Article ID 150665, 2022.

[24] C. D. Fernandes, V. R. S. Nascimento, D. B. Meneses et al., "Fungal biosynthesis of lignin-modifying enzymes from pulp wash and Luffa cylindrica for azo dye RB5 biodecolorization using modeling by response surface methodology and artificial neural network," *Journal of Hazardous Materials*, vol. 399, Article ID 123094, 2020.

[25] S. Vyas and M. Chhabra, "Isolation, identification and characterization of Cystobasidium oligophagum JRC1: a cellulase and lipase producing oleaginous yeast," *Bioresource Technology*, vol. 223, pp. 250–258, 2017.

[26] S. S. Ali, R. Al-Tohamy, R. Xie, M. M. El-Sheekh, and J. Sun, "Construction of a new lipase- and xylanase-producing oleaginous yeast consortium capable of reactive azo dye degradation and detoxification," *Bioresource Technology*, vol. 313, Article ID 123631, 2020.

[27] X. Wang, Y. Wang, S. Ning, S. Shi, and L. Tan, "Improving azo dye decolorization performance and halotolerance of pichia occidentalis A2 by static magnetic field and possible mechanisms through comparative transcriptome analysis," *Frontiers in Microbiology*, vol. 11, p. 712, 2020.

[28] E. Y. S. Soh, S. S. Lim, K. W. Chew et al., "Valorization of spent brewery yeast biosorbent with sonication-assisted adsorption for dye removal in wastewater treatment," *Environmental Research*, vol. 204, Article ID 112385, 2022.

[29] S. S. Ali, J. Sun, E. Koutra, N. El-Zawawy, T. Elsamahy, and M. El-Shetehy, "Construction of a novel cold-adapted oleaginous yeast consortium valued for textile azo dye wastewater processing and biorefinery," *Fuel*, vol. 285, Article ID 119050, 2021.

[30] H. Zhang, K. Zhang, M. Gao, Z. An, C. Tang, and X. Yan, "Degradation efficiency of the azo dye acid orange 2 and microbial community characteristics in a rotating algal biofilm reactor," *Journal of Water Process Engineering*, vol. 50, Article ID 103233, 2022.

[31] R. A. Hamouda, N. E. El-Naggar, and G. W. Abou-El-Souod, "Simultaneous bioremediation of Disperse orange-2RL Azo dye and fatty acids production by Scenedesmus obliquus cultured under mixotrophic and heterotrophic conditions," *Scientific Reports*, vol. 12, no. 1, Article ID 20768, 2022.

[32] M. M. El-Sheekh, S. M. el Shafay, A. E.-R. R. El-Shanshoury, R. Hamouda, D. Y. Gharieb, and G. W. Abou-El-Souod, "Impact of immobilized algae and its consortium in biodegradation of the textile dyes," *International Journal of Phytoremediation*, vol. 25, no. 6, pp. 687–696, 2023.

[33] S. Agrawal, D. Tipre, and S. R. Dave, "Biotreatment of azo dye containing textile industry effluent by a developed bacterial consortium immobilised on brick pieces in an indigenously designed packed bed biofilm reactor," *World Journal of Microbiology and Biotechnology*, vol. 39, no. 3, p. 83, 2023.

[34] Y. Patel and A. Gupte, "Accelerated biodecolorization and detoxification of synthetic textile dye Acid Maroon V by bacterial consortium under redox mediator system," *3 Biotech*, vol. 13, no. 2, p. 51, 2023.

[35] S. Garg and A. Roy, "Phytoremediation: an alternative approach for removal of dyes," in *Phytoremediation*, pp. 369–386, Elsevier, Amsterdam, Netherlands, 2022.

[36] G. S. Ghodake, A. A. Talke, J. P. Jadhav, and S. P. Govindwar, "Potential of BRASSICA juncea in order to treat textile—effluent—contaminated sites," *International Journal of Phytoremediation*, vol. 11, no. 4, pp. 297–312, 2009.

[37] S. E. Mbuligwe, "Comparative treatment of dye-rich wastewater in engineered wetland systems (EWSs) vegetated with different plants," *Water Research*, vol. 39, no. 2–3, pp. 271–280, 2005.

[38] M. P. Shah, "Bioremediation of azo dye," in *Microbial Wastewater Treatment*, pp. 103–126, Elsevier, Amsterdam, Netherlands, 2019.

[39] K. Paździor, L. Bilińska, and S. Ledakowicz, "A review of the existing and emerging technologies in the combination of AOPs and biological processes in industrial textile wastewater treatment," *Chemical Engineering Journal*, vol. 376, Article ID 120597, 2019.

[40] B. S. Rathi and P. S. Kumar, "Application of adsorption process for effective removal of emerging contaminants from water and wastewater," *Environmental Pollution*, vol. 280, Article ID 116995, 2021.

[41] R. Kecili and C. M. Hussain, "Mechanism of adsorption on nanomaterials," in *Nanomaterials in Chromatography*, pp. 89–115, Elsevier, Amsterdam, Netherlands, 2018.

[42] A. E. Burakov, E. V. Galunin, I. V. Burakova et al., "Adsorption of heavy metals on conventional and nanostructured materials for wastewater treatment purposes: a review," *Ecotoxicology and Environmental Safety*, vol. 148, pp. 702–712, 2018.

[43] K. G. Akpomie and J. Conradie, "Advances in application of cotton-based adsorbents for heavy metals trapping, surface modifications and future perspectives," *Ecotoxicology and Environmental Safety*, vol. 201, Article ID 110825, 2020.

[44] S. He, J. Sun, X. Jin et al., "Adsorption enhancement of Congo red dye from wastewater based on edamame shell originated activated carbon by the cations: experimental and theoretical studies," *Diamond and Related Materials*, vol. 136, Article ID 109930, 2023.

[45] F. J. Cano, O. Reyes-Vallejo, A. Ashok, M. D. L. L. Olvera, S. Velumani, and A. Kassiba, "Mechanisms of dyes adsorption on titanium oxide– graphene oxide nanocomposites," *Ceramics International*, vol. 49, no. 13, pp. 21185–21205, 2023.

[46] R. Wang, H. Cao, C. Yao et al., "Construction of alkalized MXene-supported CoFe2O4/CS composites with superstrong adsorption capacity to remove toxic dyes from aqueous solution," *Applied Surface Science*, vol. 624, Article ID 157091, 2023.

[47] Y. Zhao, H. Zhou, M. Song et al., "Interface engineering of Ti-MOFs: adsorption of anionic, cationic and neutral dyes in wastewater," *Journal of Molecular Structure*, vol. 1283, Article ID 135268, 2023.

[48] V. S. Rana and N. Sharma, "Adsorption profile of anionic and cationic dyes through Fe3O4 embedded oxidized Sterculia gum/Gelatin hybrid gel matrix," *International Journal of Biological Macromolecules*, vol. 232, Article ID 123098, 2023.

[49] K. M. A. Qasem, S. Khan, S. Chinnam et al., "Sustainable fabrication of Co-MOF@CNT nano-composite for efficient adsorption and removal of organic dyes and selective sensing of Cr(VI) in aqueous phase," *Materials Chemistry and Physics*, vol. 291, Article ID 126748, 2022.

[50] A. Belcaid, B. H. Beakou, S. Bouhsina, and A. Anouar, "New insights on manganese dioxide nanoparticles loaded on cellulose-based biochar of cassava peel for the adsorption of three cationic dyes from wastewater," *International Journal of Biological Macromolecules*, vol. 241, Article ID 124534, 2023.

[51] S. Sudan, A. Khajuria, and J. Kaushal, "Adsorption potential of pristine biochar synthesized from rice husk waste for the removal of Eriochrome black azo dye," *Materials Today: Proceedings*, vol. 44, no. 4, pp. 646–653, 2023.

[52] A. A. Khan and M. Mondal, "Effective materials in the photocatalytic treatment of dyestuffs and stained wastewater," in *Photocatalytic Degradation of Dyes*, pp. 91–111, Elsevier, Amsterdam, Netherlands, 2021.

[53] M. Wawrzkiewicz and Z. Hubicki, "Anion exchange resins as effective sorbents for removal of acid, reactive, and direct dyes from textile wastewaters," in *Ion Exchange - Studies and Applications*, InTech, Beijing, China, 2015.

[54] C. Lu, J. Yang, A. Khan, J. Yang, Q. Li, and G. Wang, "A highly efficient technique to simultaneously remove acidic and basic dyes using magnetic ion-exchange microbeads," *Journal of Environmental Management*, vol. 304, Article ID 114173, 2022.

[55] G. Bayramoglu and M. Y. Arica, "Grafting of regenerated cellulose films with fibrous polymer and modified into phosphate and sulfate groups: application for removal of a model azo-dye," *Colloids and Surfaces A: Physicochemical and Engineering Aspects*, vol. 614, Article ID 126173, 2021.

[56] N. M. Marin, L. F. Pascu, A. Demba, M. Nita-Lazar, I. A. Badea, and H. Y. Aboul-Enein, "Removal of the Acid Orange 10 by ion exchange and microbiological methods," *International journal of Environmental Science and Technology*, vol. 16, no. 10, pp. 6357–6366, 2019.

[57] J. Joseph, R. C. Radhakrishnan, J. K. Johnson, S. P. Joy, and J. Thomas, "Ion-exchange mediated removal of cationic dyestuffs from water using ammonium phosphomolybdate," *Materials Chemistry and Physics*, vol. 242, Article ID 122488, 2020.

[58] C.-Z. Liang, S.-P. Sun, F.-Y. Li, Y.-K. Ong, and T.-S. Chung, "Treatment of highly concentrated wastewater containing multiple synthetic dyes by a combined process of coagulation/flocculation and nanofiltration," *Journal of Membrane Science*, vol. 469, pp. 306–315, 2014.

[59] S. Sonal and B. K. Mishra, "Role of coagulation/flocculation technology for the treatment of dye wastewater: trend and future aspects," in *Water Pollution and Management Practices*, pp. 303–331, Springer, Singapore, 2021.

[60] A. Hadadi, A. Imessaoudene, J.-C. Bollinger et al., "Aleppo pine seeds (Pinus halepensis Mill.) as a promising novel green coagulant for the removal of Congo red dye: optimization via machine learning algorithm," *Journal of Environmental Management*, vol. 331, Article ID 117286, 2023.

[61] A. P. Shende and R. Chidambaram, "Cocoyam powder extracted from Colocasia antiquorum as a novel plant-based bioflocculant for industrial wastewater treatment: flocculation performance and mechanism," *Heliyon*, vol. 9, no. 4, Article ID 15228, 2023.

[62] S. Ihaddaden, D. Aberkane, A. Boukerroui, and D. Robert, "Removal of methylene blue (basic dye) by coagulation-flocculation with biomaterials (bentonite and Opuntia ficus indica)," *Journal of Water Process Engineering*, vol. 49, Article ID 102952, 2022.

[63] Y. Duan, J. Zhao, X. Qiu et al., "Coagulation performance and floc properties for synchronous removal of reactive dye and polyethylene terephthalate microplastics," *Process Safety and Environmental Protection*, vol. 165, pp. 66–76, 2022.

[64] I. A. Obiora-Okafo, O. D. Onukwuli, C. A. Igwegbe, C. E. Onu, and M. Omotioma, "Enhanced performance of natural polymer coagulants for dye removal from wastewater: coagulation kinetics, and mathematical modelling approach," *Environmental Processes*, vol. 9, no. 2, p. 20, 2022.

[65] R. J. Kadhim, F. H. Al-Ani, M. Al-shaeli, Q. F. Alsalhy, and A. Figoli, "Removal of dyes using graphene oxide (GO) mixed matrix membranes," *Membranes*, vol. 10, no. 12, p. 366, 2020.

[66] R. Al-Tohamy, S. S. Ali, F. Li et al., "A critical review on the treatment of dye-containing wastewater: ecotoxicological and health concerns of textile dyes and possible remediation approaches for environmental safety," *Ecotoxicology and Environmental Safety*, vol. 231, Article ID 113160, 2022.

[67] N. Li, T.-J. Lou, W. Wang et al., "MXene-PANI/PES composite ultrafiltration membranes with conductive properties for anti-fouling and dye removal," *Journal of Membrane Science*, vol. 668, Article ID 121271, 2023.

[68] A. Yusaf, M. Usman, M. Ibrahim et al., "Mixed micellar solubilization for procion blue MxR entrapment and optimization of necessary parameters for micellar enhanced ultrafiltration," *Chemosphere*, vol. 313, Article ID 137320, 2023.

[69] T. M. Subrahmanya, J. Widakdo, S. Mani et al., "An eco-friendly and reusable syringe filter membrane for the efficient removal of dyes from water via low pressure filtration assisted self-assembling of graphene oxide and SBA-15/PDA," *Journal of Cleaner Production*, vol. 349, Article ID 131425, 2022.

[70] J. Zhao, H. Liu, P. Xue et al., "High-performance PVDF water treatment membrane based on IL-Na+MMT for simultaneous removal of dyes and oil-water emulsions," *Journal of Environmental Chemical Engineering*, vol. 11, no. 1, Article ID 109093, 2023.

[71] S.-L. Li, Y. Guan, Y. Qin et al., "An antifouling loose nanofiltration membrane prepared by cross-linking HPAN ultrafiltration membrane with zwitterionic polymer PEI-CA for efficient dye desalination," *Desalination*, vol. 549, Article ID 116354, 2023.

[72] M. Dmitrenko, A. Kuzminova, A. Zolotarev et al., "Modification strategies of polyacrylonitrile ultrafiltration membrane using TiO2 for enhanced antifouling performance in water treatment," *Separation and Purification Technology*, vol. 286, Article ID 120500, 2022.

[73] S. Ahmadipouya, S. A. Mousavi, A. Shokrgozar, and D. V. Mousavi, "Improving dye removal and antifouling performance of polysulfone nanofiltration membranes by incorporation of UiO-66 metal-organic framework," *Journal of Environmental Chemical Engineering*, vol. 10, no. 3, Article ID 107535, 2022.

[74] J. Li, J.-L. Gong, S.-Y. Fang et al., "Antifouling and chemical-resistant nanofiltration membrane modulated by a functionalized MWCNT interlayer for efficient dye/salt separation at high salinity," *ACS Applied Materials & Interfaces*, vol. 15, no. 28, pp. 34272–34289, 2023.

[75] M. Li, Z. He, and J. Xu, "A comparative study of ozonation on aqueous reactive dyes and reactive-dyed cotton," *Coloration Technology*, vol. 137, no. 4, pp. 376–388, 2021.

[76] L.-B. Chu, X.-H. Xing, A.-F. Yu, Y.-N. Zhou, X.-L. Sun, and B. Jurcik, "Enhanced ozonation of simulated dyestuff wastewater by microbubbles," *Chemosphere*, vol. 68, no. 10, pp. 1854–1860, 2007.

[77] S. P. Ghuge and A. K. Saroha, "Degradation of azo dye in ozonation by noble metal supported mesoporous catalyst," *International Journal of Environment and Waste Management*, vol. 31, no. 3, p. 374, 2023.

[78] T. M. H. Le, R. Nuisin, R. Mongkolnavin, P. Painmanakul, and S. Sairiam, "Enhancing dye wastewater treatment efficiency in ozonation membrane contactors by chloro– and fluoro–organosilanes' functionality on hydrophobic PVDF membrane modification," *Separation and Purification Technology*, vol. 288, Article ID 120711, 2022.

[79] U. Y. Qazi, R. Iftikhar, A. Ikhlaq et al., "Application of Fe-RGO for the removal of dyes by catalytic ozonation process," *Environmental Science and Pollution Research*, vol. 29, no. 59, pp. 89485–89497, 2022.

[80] N. Dabuth, S. Thuangchon, T. Prasert, V. Yuthawong, and P. Phungsai, "Effects of catalytic ozonation catalyzed by TiO2 activated carbon and biochar on dissolved organic matter removal and disinfection by-product formations investigated by Orbitrap mass spectrometry," *Journal of Environmental Chemical Engineering*, vol. 10, no. 2, Article ID 107215, 2022.

[81] M. Zajda and U. Aleksander-Kwaterczak, "Wastewater treatment methods for effluents from the confectionery industry – an overview," *Journal of Ecological Engineering*, vol. 20, no. 9, pp. 293–304, 2019.

[82] M. Eyvaz, M. Kirlaroglu, T. S. Aktas, and E. Yuksel, "The effects of alternating current electrocoagulation on dye removal from aqueous solutions," *Chemical Engineering Journal*, vol. 153, no. 1–3, pp. 16–22, 2009.

[83] A. A. Márquez, O. Coreño, and J. L. Nava, "Removal of brilliant green tannery dye by electrocoagulation," *Journal of Electroanalytical Chemistry*, vol. 911, Article ID 116223, 2022.

[84] C. E. Lach, C. S. Pauli, A. S. Coan, E. L. Simionatto, and L. A. D. Koslowski, "Investigating the process of electrocoagulation in the removal of azo dye from synthetic textile effluents and the effects of acute toxicity on Daphnia magna test organisms," *Journal of Water Process Engineering*, vol. 45, Article ID 102485, 2022.

[85] Y. Liu, C. Li, J. Bao, X. Wang, W. Yu, and L. Shao, "Degradation of azo dyes with different functional groups in simulated wastewater by electrocoagulation," *Water*, vol. 14, no. 1, p. 123, 2022.

[86] J. Yao, L. Wang, G. Zhang, J. Tao, X. Shi, and F. Wei, "Plate structure optimization and performance study of a new continuous flow electrocoagulation reactor," *Chemical Engineering Research and Design*, vol. 194, pp. 693–704, 2023.

[87] I. A. Ahmed, S. A. Nosier, G. F. Malash et al., "Removal of brilliant yellow azo dye from wastewater by electrocoagulation in a cell of improved design," *Water, Air, & Soil Pollution*, vol. 234, no. 4, p. 237, 2023.

[88] K. Hendaoui, M. Trabelsi-Ayadi, and F. Ayari, "Optimization and mechanisms analysis of indigo dye removal using continuous electrocoagulation," *Chinese Journal of Chemical Engineering*, vol. 29, pp. 242–252, 2021.

[89] V. V. Kuokkanen, "Water treatment by electrocoagulation," in *Encyclopedia of Inorganic and Bioinorganic Chemistry*, pp. 1–12, John Wiley & Sons, Ltd, Ontario, UK, 2016.

[90] M. Saleh, Z. Bilici, M. Kaya et al., "The use of basalt powder as a natural heterogeneous catalyst in the Fenton and Photo-Fenton oxidation of cationic dyes," *Advanced Powder Technology*, vol. 32, no. 4, pp. 1264–1275, 2021.

[91] O. Eskikaya, Z. Isik, C. Arslantas et al., "Preparation of hydrochar bio-based catalyst for fenton process in dye-containing wastewater treatment," *Environmental Research*, vol. 216, Article ID 114357, 2023.

[92] S. B. Ayed, L. Mansour, V. Vaiano, A. Halim Harrath, F. Ayari, and L. Rizzo, "Magnetic Fe3O4-natural iron ore/calcium alginate beads as heterogeneous catalyst for Novacron blue dye degradation in water by (photo)Fenton process," *Journal of Photochemistry and Photobiology A: Chemistry*, vol. 438, Article ID 114566, 2023.

[93] B. Jain, A. Hashmi, S. Sanwaria, A. K. Singh, M. A. B. H. Susan, and A. Singh, "Zinc oxide nanoparticle incorporated on graphene oxide: an efficient and stable photocatalyst for water treatment through the Fenton process," *Advanced Composites and Hybrid Material*, vol. 3, no. 2, pp. 231–242, 2020.

[94] J. Tang, R. Xu, G. Sui et al., "Double-shelled porous g-C3N4 nanotubes modified with amorphous Cu-doped FeOOH nanoclusters as 0D/3D non-homogeneous photo-fenton catalysts for effective removal of organic dyes," *Small*, vol. 19, no. 22, Article ID 2208232, 2023.

[95] J. Wei, W. Shen, and Y. Liu, "Facile synthesis of SrWO4@MIL-88A(Fe) heterojunctions and their deep treatment of dye wastewater and municipal landfill leachate using photo-Fenton technology," *Journal of Industrial and Engineering Chemistry*, vol. 120, pp. 103–120, 2023.

[96] N. Dai, S. Yi, X. Zhang et al., "Typical synthesis of an iron-modified Laponite @diatomite composite for photo-Fenton degradation of methyl orange dyes," *Applied Surface Science*, vol. 607, Article ID 154886, 2023.

[97] H. Fakhri and M. Farzadkia, "Nanophotocatalysts for biodegradation of materials," in *Biodegradation and Biodeterioration at the Nanoscale*, pp. 85–103, Elsevier, Amsterdam, Netherlands, 2022.

[98] C. F. Goodeve and J. A. Kitchener, "The mechanism of photosensitisation by solids," *Transactions of the Faraday Society*, vol. 34, p. 902, 1938.

[99] R. Ameta, M. S. Solanki, S. Benjamin, and S. C. Ameta, "Photocatalysis," in *Advanced Oxidation Processes for Waste Water Treatment*, pp. 135–175, Elsevier, Amsterdam, Netherlands, 2018.

[100] S. Irfan, Z. Zhuanghao, F. Li et al., "Critical review: bismuth ferrite as an emerging visible light active nanostructured photocatalyst," *Journal of Materials Research and Technology*, vol. 8, no. 6, pp. 6375–6389, 2019.

[101] R. M. Abu Shmeis, "Nanotechnology in wastewater treatment," 2022, https://www.intechopen.com/chapters/78696.

[102] M. Devi, S. Praharaj, and D. Rout, "Industrial problems and solution towards visible light photocatalysis," in *Nanostructured Materials for Visible Light Photocatalysis*, pp. 535–567, Elsevier, Amsterdam, Netherlands, 2022.

[103] H. Wang, L. Zhang, Z. Chen et al., "Semiconductor heterojunction photocatalysts: design, construction, and photocatalytic performances," *Chemical Society Reviews*, vol. 43, no. 15, p. 5234, 2014.

[104] J. Low, J. Yu, M. Jaroniec, S. Wageh, and A. A. Al-Ghamdi, "Heterojunction photocatalysts," *Advanced Materials*, vol. 29, no. 20, 2017.

[105] S. N. Ahmed and W. Haider, "Heterogeneous photocatalysis and its potential applications in water and wastewater treatment: a review," *Nanotechnology*, vol. 29, no. 34, Article ID 342001, 2018.

[106] I. Y. Kim, Y. K. Jo, J. M. Lee, L. Wang, and S.-J. Hwang, "Unique advantages of exfoliated 2D nanosheets for tailoring the functionalities of nanocomposites," *The Journal of Physical Chemistry Letters*, vol. 5, no. 23, pp. 4149–4161, 2014.

[107] B. Roul, M. Kumar, M. K. Rajpalke, T. N. Bhat, and S. B. Krupanidhi, "Binary group III-nitride based heterostructures: band offsets and transport properties," *Journal of*

Physics D: Applied Physics, vol. 48, no. 42, Article ID 423001, 2015.

[108] Q. Xu, L. Zhang, J. Yu, S. Wageh, A. A. Al-Ghamdi, and M. Jaroniec, "Direct Z-scheme photocatalysts: principles, synthesis, and applications," *Materials Today*, vol. 21, no. 10, pp. 1042–1063, 2018.

[109] T. Jiang, A. S. Poyraz, A. Iyer et al., "Synthesis of mesoporous iron oxides by an inverse micelle method and their application in the degradation of orange II under visible light at neutral pH," *Journal of Physical Chemistry C*, vol. 119, no. 19, pp. 10454–10468, 2015.

[110] C. Liang, H. Liu, J. Zhou, X. Peng, and H. Zhang, "One-step synthesis of spherical γ-Fe 2 O 3 nanopowders and the evaluation of their photocatalytic activity for orange I degradation," *Journal of Chemistry*, vol. 2015, Article ID 791829, 8 pages, 2015.

[111] S. Karthikeyeni, T. Siva Vijayakumar, S. Vasanth et al., "Decolourisation of Direct Orange S dye by ultra sonication using iron oxide nanoparticles," *Journal of Experimental Nanoscience*, vol. 10, no. 3, pp. 199–208, 2015.

[112] P. Sharma, D. S. Rana, A. Umar et al., "Iron oxide nanocubes for photocatalytic degradation and antimicrobial applications," *Nanoscience and Nanotechnology Letters*, vol. 8, no. 11, pp. 1014–1019, 2016.

[113] H. R. Ali, H. N. Nassar, and N. S. El-Gendy, "Green synthesis of α-Fe_2O_3 using *Citrus reticulum* peels extract and water decontamination from different organic pollutants," *Energy Sources, Part A: Recovery, Utilization, and Environmental Effects*, vol. 39, no. 13, pp. 1425–1434, 2017.

[114] C. Xiao, J. Li, and G. Zhang, "Synthesis of stable burger-like α-Fe2O3 catalysts: formation mechanism and excellent photo-Fenton catalytic performance," *Journal of Cleaner Production*, vol. 180, pp. 550–559, 2018.

[115] G. K. Weldegebrieal and A. K. Sibhatu, "Photocatalytic activity of biosynthesized α-Fe2O3 nanoparticles for the degradation of methylene blue and methyl orange dyes," *Optik*, vol. 241, Article ID 167226, 2021.

[116] N. K. Gupta, Y. Ghaffari, J. Bae, and K. S. Kim, "Synthesis of coral-like α-Fe2O3 nanoparticles for dye degradation at neutral pH," *Journal of Molecular Liquids*, vol. 301, Article ID 112473, 2020.

[117] R. K. Shah, "Efficient photocatalytic degradation of methyl orange dye using facilely synthesized α-Fe2O3 nanoparticles," *Arabian Journal of Chemistry*, vol. 16, no. 2, Article ID 104444, 2023.

[118] M. U. D. Sheikh, G. A. Naikoo, M. Thomas, M. Bano, and F. Khan, "Solar-assisted photocatalytic reduction of methyl orange azo dye over porous TiO 2 nanostructures," *New Journal of Chemistry*, vol. 40, no. 6, pp. 5483–5494, 2016.

[119] N. S. Allen, N. Mahdjoub, V. Vishnyakov, P. J. Kelly, and R. J. Kriek, "The effect of crystalline phase (anatase, brookite and rutile) and size on the photocatalytic activity of calcined polymorphic titanium dioxide (TiO 2)," *Polymer Degradation and Stability*, vol. 150, pp. 31–36, 2018.

[120] R. B. Rajput and R. B. Kale, "The facile synthesis of 3D hierarchical flower-like TiO2 microspheres with enhanced photocatalytic activity," *Journal of Physics and Chemistry of Solids*, vol. 177, Article ID 111286, 2023.

[121] D. P. Dave and K. V. Chauhan, "Synthesis of visible spectrum-active TiO2 thin film induced by RF magnetron sputtering," *Materials Today: Proceedings*, vol. 62, pp. 4254–4259, 2022.

[122] O. Secundino-Sánchez, J. Díaz-Reyes, J. F. Sánchez-Ramírez, J. S. Arias-Cerón, M. Galván-Arellano, and O. Vázquez-Cuchillo, "Controlled synthesis of electrospun TiO2 nanofibers and their photocatalytic application in the decolouration of Remazol Black B azo dye," *Catalysis Today*, vol. 392-393, pp. 13–22, 2022.

[123] S. Saensook and A. Sirisuk, "A factorial experimental design approach to obtain defect-rich black TiO2 for photocatalytic dye degradation," *Journal of Water Process Engineering*, vol. 45, Article ID 102495, 2022.

[124] L. Mais, A. Vacca, M. Mascia, E. M. Usai, S. Tronci, and S. Palmas, "Experimental study on the optimisation of azo-dyes removal by photo-electrochemical oxidation with TiO2 nanotubes," *Chemosphere*, vol. 248, Article ID 125938, 2020.

[125] Z. M. Redha, H. Abdulla Yusuf, R. Amin, and M. Bououdina, "The study of photocatalytic degradation of a commercial azo reactive dye in a simple design reusable miniaturized reactor with interchangeable TiO 2 nanofilm," *Arab Journal of Basic and Applied Sciences*, vol. 27, no. 1, pp. 287–298, 2020.

[126] K. Lingaraju, H. R. Naika, K. Manjunath, G. Nagaraju, D. Suresh, and H. Nagabhushana, "Rauvolfia serpentina-mediated green synthesis of CuO nanoparticles and its multidisciplinary studies," *Acta Metallurgica Sinica*, vol. 28, no. 9, pp. 1134–1140, 2015.

[127] V. Scuderi, G. Amiard, S. Boninelli et al., "Photocatalytic activity of CuO and Cu2O nanowires," *Materials Science in Semiconductor Processing*, vol. 42, pp. 89–93, 2016.

[128] A. A. Novikova, D. Y. Moiseeva, E. V. Karyukov, and A. A. Kalinichenko, "Facile preparation photocatalytically active CuO plate-like nanoparticles from brochantite," *Materials Letters*, vol. 167, pp. 165–169, 2016.

[129] K. Alsamhary, N. M. Al-Enazi, E. Alhomaidi, and S. Alwakeel, "Spirulina platensis mediated biosynthesis of Cuo Nps and photocatalytic degradation of toxic azo dye Congo red and kinetic studies," *Environmental Research*, vol. 207, Article ID 112172, 2022.

[130] S. Aroob, S. A. C. Carabineiro, M. B. Taj et al., "Green synthesis and photocatalytic dye degradation activity of CuO nanoparticles," *Catalysts*, vol. 13, no. 3, p. 502, 2023.

[131] B. Polat, Z. Bilici, Y. Ozay, I. Kucukkara, and N. Dizge, "Photocatalytic decolorization of BR18 and RR180 dyes by semiconductor diode laser using CuO for wastewater treatment," *Water, Air, & Soil Pollution*, vol. 233, no. 8, p. 316, 2022.

[132] S. A. Bhat, F. Zafar, A. H. Mondal et al., "Photocatalytic degradation of carcinogenic Congo red dye in aqueous solution, antioxidant activity and bactericidal effect of NiO nanoparticles," *Journal of the Iranian Chemical Society*, vol. 17, no. 1, pp. 215–227, 2020.

[133] Z. Sabouri, A. Akbari, H. A. Hosseini, M. Khatami, and M. Darroudi, "Tragacanth-mediate synthesis of NiO nanosheets for cytotoxicity and photocatalytic degradation of organic dyes," *Bioprocess and Biosystems Engineering*, vol. 43, no. 7, pp. 1209–1218, 2020.

[134] W. Sun, L. Xiao, and X. Wu, "Facile synthesis of NiO nanocubes for photocatalysts and supercapacitor electrodes," *Journal of Alloys and Compounds*, vol. 772, pp. 465–471, 2019.

[135] S. M. Roopan, G. Elango, D. D. Priya et al., "Sunlight mediated photocatalytic degradation of organic pollutants by statistical optimization of green synthesized NiO NPs as catalyst," *Journal of Molecular Liquids*, vol. 293, Article ID 111509, 2019.

[136] X. Chen, Z. Wu, D. Liu, and Z. Gao, "Preparation of ZnO photocatalyst for the efficient and rapid photocatalytic

degradation of azo dyes," *Nanoscale Research Letters*, vol. 12, no. 1, p. 143, 2017.

[137] S. Sakthivel, B. Neppolian, M. V. Shankar, B. Arabindoo, M. Palanichamy, and V. Murugesan, "Solar photocatalytic degradation of azo dye: comparison of photocatalytic efficiency of ZnO and TiO2," *Solar Energy Materials and Solar Cells*, vol. 77, no. 1, pp. 65–82, 2003.

[138] S. A. Al-Zahrani, M. B. Patil, S. N. Mathad et al., "Photocatalytic degradation of textile orange 16 reactive dye by ZnO nanoparticles synthesized via green route using punica granatum leaf extract," *Crystals*, vol. 13, no. 2, p. 172, 2023.

[139] M. F. Lanjwani, M. Y. Khuhawar, T. M. J. Khuhawar et al., "Photocatalytic degradation of eriochrome black T dye by ZnO nanoparticles using multivariate factorial, kinetics and isotherm models," *Journal of Cluster Science*, vol. 34, no. 2, pp. 1121–1132, 2023.

[140] S. M. Saleh, "ZnO nanospheres based simple hydrothermal route for photocatalytic degradation of azo dye," *Spectrochimica Acta Part A: Molecular and Biomolecular Spectroscopy*, vol. 211, pp. 141–147, 2019.

[141] T. Sansenya, N. Masri, T. Chankhanittha et al., "Hydrothermal synthesis of ZnO photocatalyst for detoxification of anionic azo dyes and antibiotic," *Journal of Physics and Chemistry of Solids*, vol. 160, Article ID 110353, 2022.

[142] K. Umar, M. F. B. Mfarrej, Q. I. Rahman et al., "ZnO Nanoswirlings for Azo Dye AR183 photocatalytic degradation and antimycotic activity," *Scientific Reports*, vol. 12, no. 1, Article ID 14023, 2022.

[143] K.-Y. A. Lin and T.-Y. Lin, "Degradation of acid azo dyes using oxone activated by cobalt titanate perovskite," *Water, Air, & Soil Pollution*, vol. 229, no. 1, p. 10, 2018.

[144] A. R. F. A. Teixeira, A. de Meireles Neris, E. Longo et al., "SrSnO3 perovskite obtained by the modified Pechini method—insights about its photocatalytic activity," *Journal of Photochemistry and Photobiology A: Chemistry*, vol. 369, pp. 181–188, 2019.

[145] M. C. Maridevaru, B. Aljafari, S. Anandan, and M. Ashokkumar, "Synergistic impacts of sonolysis aided photocatalytic degradation of water pollutant over perovskite-type CeNiO3 nanospheres," *New Journal of Chemistry*, vol. 46, no. 21, pp. 10117–10127, 2022.

[146] S. Merrad, M. Abbas, R. Brahimi, and M. Trari, "Study of Congo Red removal from aqueous solution by using the deficient perovskite SrTiO3-δ under solar light," *Journal of Molecular Structure*, vol. 1265, Article ID 133349, 2022.

[147] M. C. Maridevaru, J. J. Wu, R. Viswanathan Mangalaraja, and S. Anandan, "Ultrasonic-assisted preparation of perovskite-type lanthanum nickelate nanostructures and its photocatalytic properties," *ChemistrySelect*, vol. 5, no. 26, pp. 7947–7958, 2020.

[148] B. Palas, G. Ersöz, and S. Atalay, "Catalytic wet air oxidation of Reactive Black 5 in the presence of LaNiO3 perovskite catalyst as a green process for azo dye removal," *Chemosphere*, vol. 209, pp. 823–830, 2018.

[149] M. B. Taj, M. D. F. Alkahtani, A. Raheel et al., "Bioconjugate synthesis, phytochemical analysis, and optical activity of NiFe2O4 nanoparticles for the removal of ciprofloxacin and Congo red from water," *Scientific Reports*, vol. 11, no. 1, p. 5439, 2021.

[150] N. M. Mahmoodi, "Manganese ferrite nanoparticle: synthesis, characterization, and photocatalytic dye degradation ability," *Desalination and Water Treatment*, vol. 53, no. 1, pp. 84–90, 2015.

[151] J. Ćirković, A. Radojković, D. Luković Golić et al., "Visible-light photocatalytic degradation of Mordant Blue 9 by single-phase BiFeO3 nanoparticles," *Journal of Environmental Chemical Engineering*, vol. 9, no. 1, Article ID 104587, 2021.

[152] P. Dhiman, T. Mehta, A. Kumar et al., "Mg0.5NixZn0.5-xFe2O4 spinel as a sustainable magnetic nano-photocatalyst with dopant driven band shifting and reduced recombination for visible and solar degradation of Reactive Blue-19," *Advanced Powder Technology*, vol. 31, no. 12, pp. 4585–4597, 2020.

[153] C. Cai, J. Liu, Z. Zhang, Y. Zheng, and H. Zhang, "Visible light enhanced heterogeneous photo-degradation of Orange II by zinc ferrite (ZnFe2O4) catalyst with the assistance of persulfate," *Separation and Purification Technology*, vol. 165, pp. 42–52, 2016.

[154] G. Ramadoss, S. P. Suriyaraj, R. Sivaramakrishnan, A. Pugazhendhi, and S. Rajendran, "Mesoporous ferromagnetic manganese ferrite nanoparticles for enhanced visible light mineralization of azoic dye into nontoxic by-products," *Science of the Total Environment*, vol. 765, Article ID 142707, 2021.

[155] R. A. El-Salamony, W. A. Aboutaleb, and A. S. Dhmees, "Photodegradation of amido black 10b dye under visible light using Ni and Zn ferrite catalysts prepared by a simple modified sol–gel method," *Arabian Journal for Science and Engineering*, vol. 48, no. 6, pp. 7661–7672, 2023.

[156] D. Sun, T. Wang, Y. Xu, R. Li, and T. Sato, "Hierarchical bismuth oxychlorides constructed by porous nanosheets: preparation, growth mechanism, and application in photocatalysis," *Materials Science in Semiconductor Processing*, vol. 31, pp. 666–677, 2015.

[157] X. Wang, F. Li, D. Li, R. Liu, and S. Liu, "Facile synthesis of flower-like BiOI hierarchical spheres at room temperature with high visible-light photocatalytic activity," *Materials Science and Engineering: B*, vol. 193, pp. 112–120, 2015.

[158] A. C. Mera, H. Váldes, F. J. Jamett, and M. F. Meléndrez, "BiOBr microspheres for photocatalytic degradation of an anionic dye," *Solid State Sciences*, vol. 65, pp. 15–21, 2017.

[159] M. Nourzad, A. Dehghan, Z. Niazi et al., "Low power photo-assisted catalytic degradation of azo dyes using 1-D BiOI: optimization of the key physicochemical features," *Catalysis Communications*, vol. 174, Article ID 106567, 2023.

[160] H. Yu and Q. Han, "Effect of reaction mediums on photocatalytic performance of BiOX (X = Cl, Br, I)," *Optical Materials*, vol. 119, Article ID 111399, 2021.

[161] L. N. Mendez-Alvarado, A. Medina-Ramirez, J. Manriquez, R. Navarro-Mendoza, R. Fuentes-Ramirez, and J. M. Peralta-Hernandez, "Synthesis of microspherical structures of bismuth oxychloride (BiOCl) towards the degradation of reactive orange 84 dye with sunlight," *Materials Science in Semiconductor Processing*, vol. 114, Article ID 105086, 2020.

[162] K. C. Christoforidis, T. Montini, E. Bontempi, S. Zafeiratos, J. J. D. Jaén, and P. P. Fornasiero, "Synthesis and photocatalytic application of visible-light active β-Fe 2 O 3/g-C 3 N 4 hybrid nanocomposites," *Applied Catalysis B: Environmental*, vol. 187, pp. 171–180, 2016.

[163] A. P. Kumar, D. Bilehal, T. Desalegn et al., "Studies on synthesis and characterization of Fe3O4@SiO2@Ru hybrid magnetic composites for reusable photocatalytic application," *Adsorption Science and Technology*, vol. 2022, Article ID 3970287, 18 pages, 2022.

[164] G. Palanisamy, T. Pazhanivel, K. Bhuvaneswari, G. Bharathi, G. Marimuthu, and T. Maiyalagan, "Spinel oxide ZnCr2O4 incorporated with ZnS quantum dots for application on

visible light driven photocatalyst Azo dye degradation," *Colloids and Surfaces A: Physicochemical and Engineering Aspects*, vol. 590, Article ID 124505, 2020.

[165] R. Malik, P. S. Rana, V. K. Tomer, V. Chaudhary, S. P. Nehra, and S. Duhan, "Nano gold supported on ordered mesoporous WO3/SBA-15 hybrid nanocomposite for oxidative decolorization of azo dye," *Microporous and Mesoporous Materials*, vol. 225, pp. 245–254, 2016.

[166] M. B. R. Aiello, G. C. Lavorato, J. C. Azcárate et al., "Magnetic nanoparticle–polymer composites loaded with hydrophobic sensitizers for photodegradation of azoic dyes," *American Chemical Society Applied Nano Materials*, vol. 5, no. 5, pp. 7460–7470, 2022.

[167] S. Fatima and S. Rizwan, "Synergetic catalytic and photocatalytic performances of tin-doped BiFeO 3/graphene nanoplatelet hybrids under dark and light conditions," *American Chemical Society Omega*, vol. 8, no. 4, pp. 3736–3744, 2023.

[168] S. J. Pradeeba, K. Sampath, and A. Ramadevi, "Photocatalytic degradations of methylene blue, malachite green and Bismarck brown using poly(azomethine)/TiO2 nanocomposite," *Cluster Computing*, vol. 22, no. 2, pp. 3893–3909, 2019.

[169] S. Ravikumar, D. Mani, E. Chicardi et al., "Development of highly efficient cost-effective CdS/Ag nanocomposite for removal of azo dyes under UV and solar light," *Ceramics International*, vol. 49, no. 6, pp. 9551–9559, 2023.

[170] X. Yang, Z. Luo, D. Wang, C. Deng, Y. Zhao, and F. Tang, "Simple hydrothermal preparation of sulfur fluoride-doped g-C3N4 and its photocatalytic degradation of methyl orange," *Materials Science and Engineering: B*, vol. 288, Article ID 116216, 2023.

[171] R. Ranjithkumar, C. van Nguyen, L. S. Wong et al., "Chitosan functionalized bismuth oxychloride/zinc oxide nanocomposite for enhanced photocatalytic degradation of Congo red," *International Journal of Biological Macromolecules*, vol. 225, pp. 103–111, 2023.

[172] H. Zhang, D. Zhang, D. Zhang et al., "High-performance integrated rGO-[polymeric ionic liquid] [heteropolyanions] for catalytic degradation of azo dyes," *Langmuir*, vol. 39, no. 2, pp. 739–749, 2023.

[173] F. S. Razavi, D. Ghanbari, E. A. Dawi, and M. Salavati-Niasari, "Electrospun bimetallic Au–Pt/TiO2/BaFe12O19 nanofibers as promising photocatalysts driven by visible light: synthesis and characterization," *Journal of Science: Advanced Materials and Devices*, vol. 8, no. 2, Article ID 100559, 2023.

[174] Y.-C. Liu, X. Liu, X. Wang, Z.-H. Li, C.-L. Chen, and Z. Xiang, "Hybrid persulfate/sonocatalysis for degradation of acid orange 7 in the presence of Ag2O/CuWO4 composite: operating parameters and sonocatalytic mechanism," *Journal of Cleaner Production*, vol. 394, Article ID 136287, 2023.

[175] H. A. Abubshait, M. Saad, S. Iqbal et al., "Co-doped zinc oxide nanoparticles embedded in Polyvinylalcohol Hydrogel as solar light derived photocatalyst disinfection and removal of coloured pollutants," *Journal of Molecular Structure*, vol. 1271, Article ID 134100, 2023.

[176] Y. Kang, B. Zhang, J. Miao et al., "Superparamagnetic Fe3O4@Al-basedmetal-organic framework nanocomposites with high-performance removal of Congo red," *Journal of Environmental Chemical Engineering*, vol. 11, no. 3, Article ID 109754, 2023.

[177] A. Mukherjee, B. Panda, D. Mondal et al., "Mesoporous, phase-pure Al3+ engrafted spinel ZnAlxB2−xO4 x= 0, 1;B= Cr3+/Fe3+ for effective fluoride chemisorption and photodegradation of azo/non-azo dyes," *Journal of Environmental Chemical Engineering*, vol. 11, no. 1, Article ID 109237, 2023.

[178] T. Gul, S. Ahmad, I. Khan et al., "Photodegradation of orange II dye using p-n junction NiO/TiO2 composite, and assessment of its biological activities," *Journal of Saudi Chemical Society*, vol. 27, no. 4, Article ID 101654, 2023.

[179] S. S. Mukonza, N. Chaukura, and A. K. Mishra, "Photocatalytic activity and reusability of F, Sm3+ Co-doped TiO2/MWCNTs hybrid heterostructure for efficient photocatalytic degradation of brilliant black bis-azo dye," *Catalysts*, vol. 13, no. 1, p. 86, 2022.

[180] T. J. Al-Musawi, G. McKay, P. Rajiv, N. Mengelizadeh, and D. Balarak, "Efficient sonophotocatalytic degradation of acid blue 113 dye using a hybrid nanocomposite of CoFe2O4 nanoparticles loaded on multi-walled carbon nanotubes," *Journal of Photochemistry and Photobiology A: Chemistry*, vol. 424, Article ID 113617, 2022.

[181] V. Ramasubbu, P. Ram Kumar, T. Chellapandi, G. Madhumitha, E. M. Mothi, and X. S. Shajan, "Zn(II) porphyrin sensitized (TiO2@Cd-MOF) nanocomposite aerogel as novel photocatalyst for the effective degradation of methyl orange (MO) dye," *Optical Materials*, vol. 132, Article ID 112558, 2022.

[182] E. Yilmaz, S. Salem, G. Sarp et al., "TiO2 nanoparticles and C-Nanofibers modified magnetic Fe3O4 nanospheres (TiO2@Fe3O4@C–NF): a multifunctional hybrid material for magnetic solid-phase extraction of ibuprofen and photocatalytic degradation of drug molecules and azo dye," *Talanta*, vol. 213, Article ID 120813, 2020.

[183] M. Kardeş, H. C. Yatmaz, and K. Öztürk, "ZnO nanorods grown on flexible polyurethane foam surfaces for photocatalytic azo dye treatment," *American Chemical Society Applied Nano Materials*, vol. 6, no. 8, pp. 6605–6613, 2023.

[184] M. Ishfaq, M. Aadil, S. R. Ejaz et al., "Synthesis of binary metal doped CeO2 via the subcritical hydrothermal method for photo-mineralizing methyl orange dye," *Journal of Alloys and Compounds*, vol. 960, Article ID 170661, 2023.

[185] U. M. Nisha, M. N. Meeran, R. Sethupathi, V. Subha, P. Rajeswaran, and P. Sivakarthik, "Studies on Chitosan modified ZrO2–CeO2 metal oxide and their Photo catalytic activity under solar light irradiation for water remediation," *Journal of the Indian Chemical Society*, vol. 100, no. 8, Article ID 101061, 2023.

[186] Z.-H. Zhang and Y.-J. Shih, "Solar-light-sensitive applications of recycled iron oxyhydroxide as photoelectrolytic heterostructure by encapsulating in reduced graphene oxide and titanium oxide nanotube array (FeOxrGO/TiNTA)," *Separation and Purification Technology*, vol. 323, Article ID 124407, 2023.

[187] Q. Zou, Z. Zhu, and Z. Yuan, "Bimetallic FeNi alloy nanoparticles grown on graphene for efficient removal of Congo red from aqueous solution," *Advanced Sustainable Systems*, vol. 7, no. 3, Article ID 2200405, 2023.

[188] L. T. Thao, T. V. Nguyen, V. Q. Nguyen et al., "Orange G degradation by heterogeneous peroxymonosulfate activation based on magnetic MnFe2O4/α-MnO2 hybrid," *Journal of Environmental Sciences*, vol. 124, pp. 379–396, 2023.

[189] A. P. Chowdhury, K. S. Anantharaju, S. S. Umare, and S. S. Dhar, "Facile fabrication of binary BiOCl-Cu2CoSnS4 and ternary BiOCl-Cu2CoSnS4-TiO2 heterojunction nano photocatalyst for efficient sunlight-driven removal of direct blue 71 in an aqueous medium," *Colloids and Surfaces A:*

Physicochemical and Engineering Aspects, vol. 652, Article ID 129841, 2022.

[190] H. P. Gogoi, G. Bisoi, P. Barman, A. Dehingia, S. Das, and A. P. Chowdhury, "Highly efficient and recyclable quaternary Ag/Ag3PO4–BiOBr–C3N4 composite fabrication for efficient solar-driven photocatalytic performance for anionic pollutant in an aqueous medium and mechanism insights," *Optical Materials*, vol. 138, Article ID 113712, 2023.

[191] P. Borthakur, P. K. Boruah, N. Hussain, Y. Silla, and M. R. Das, "Specific ion effect on the surface properties of Ag/reduced graphene oxide nanocomposite and its influence on photocatalytic efficiency towards azo dye degradation," *Applied Surface Science*, vol. 423, pp. 752–761, 2017.

[192] H. Mittal and M. Khanuja, "Optimization of MoSe2 nanostructure by surface modification using conducting polymer for degradation of cationic and anionic dye: photocatalysis mechanism, reaction kinetics and intermediate product study," *Dyes and Pigments*, vol. 175, Article ID 108109, 2020.

[193] P. Borthakur and M. R. Das, "Hydrothermal assisted decoration of NiS2 and CoS nanoparticles on the reduced graphene oxide nanosheets for sunlight driven photocatalytic degradation of azo dye: effect of background electrolyte and surface charge," *Journal of Colloid and Interface Science*, vol. 516, pp. 342–354, 2018.

[194] S. Verma, B. Tirumala Rao, R. Singh, and R. Kaul, "Photocatalytic degradation kinetics of cationic and anionic dyes using Au–ZnO nanorods: role of pH for selective and simultaneous degradation of binary dye mixtures," *Ceramics International*, vol. 47, no. 24, pp. 34751–34764, 2021.

[195] A. Rafiq, M. Ikram, S. Ali et al., "Photocatalytic degradation of dyes using semiconductor photocatalysts to clean industrial water pollution," *Journal of Industrial and Engineering Chemistry*, vol. 97, pp. 111–128, 2021.

[196] A. Akbari, Z. Sabouri, H. A. Hosseini, A. Hashemzadeh, M. Khatami, and M. Darroudi, "Effect of nickel oxide nanoparticles as a photocatalyst in dyes degradation and evaluation of effective parameters in their removal from aqueous environments," *Inorganic Chemistry Communications*, vol. 115, Article ID 107867, 2020.

[197] A. Gnanaprakasam, V. M. Sivakumar, and M. Thirumarimurugan, "Influencing parameters in the photocatalytic degradation of organic effluent via nanometal oxide catalyst: a review," *Indian Journal of Materials Science*, vol. 2015, Article ID 601827, 16 pages, 2015.

[198] M. Hasanpour and M. Hatami, "Photocatalytic performance of aerogels for organic dyes removal from wastewaters: review study," *Journal of Molecular Liquids*, vol. 309, Article ID 113094, 2020.

[199] J. Zhang, B. Tian, L. Wang, M. Xing, and J. Lei, "Mechanism of photocatalysis," *Advanced Oxidation Processes for Waste Water Treatment*, pp. 1–15, 2018.

[200] M.-J. Gao, X.-D. Wang, M. Guo, and M. Zhang, "Contrast on COD photo-degradation in coking wastewater catalyzed by TiO2 and TiO2–TiO2 nanorod arrays," *Catalysis Today*, vol. 174, no. 1, pp. 79–87, 2011.

[201] T. A. Saleh, M. A. Gondal, Q. A. Drmosh, Z. H. Yamani, and A. Al-yamani, "Enhancement in photocatalytic activity for acetaldehyde removal by embedding ZnO nano particles on multiwall carbon nanotubes," *Chemical Engineering Journal*, vol. 166, no. 1, pp. 407–412, 2011.

[202] D. F. Ollis, E. Pelizzetti, and N. Serpone, "Photocatalyzed destruction of water contaminants," *Environmental Science and Technology*, vol. 25, no. 9, pp. 1522–1529, 1991.

[203] D. C. D. S. Alves, B. S. de Farias, C. Breslin, L. A. D. A. Pinto, and T. R. S. Cadaval, "Carbon nanotube-based materials for environmental remediation processes," in *Advanced Materials for Sustainable Environmental Remediation*, pp. 475–513, Elsevier, Amsterdam, Netherlands, 2022.

[204] A. Paul Chowdhury and B. H. Shambharkar, "Synthesis and characterization of BiOCl-CoWO 4 nanocomposites with improved photocatalytic activity," *International Journal of Applied Ceramic Technology*, vol. 17, no. 3, pp. 1467–1478, 2020.

[205] A. Paul Chowdhury and B. H. Shambharkar, "Synthesis and photocatalytic properties of sunlight-responsive BiOBr–CoWO 4 heterostructured nanocomposites," *Applied Organometallic Chemistry*, vol. 34, no. 4, 2020.

[206] V. Múčka, P. Bláha, V. Čuba, and J. Červenák, "Influence of various scavengers of •OH radicals on the radiation sensitivity of yeast and bacteria," *International Journal of Radiation Biology*, vol. 89, no. 12, pp. 1045–1052, 2013.

[207] J. M. Montoya-Zamora, A. Martínez-de la Cruz, E. López-Cuéllar, and F. A. Pérez González, "BiOBr photocatalyst with high activity for NOx elimination," *Advanced Powder Technology*, vol. 31, no. 8, pp. 3618–3627, 2020.

[208] H. Zhou, W. Qu, M. Wu et al., "Synthesis of novel BiOBr/Bio-veins composite for photocatalytic degradation of pollutants under visible-light," *Surfaces and Interfaces*, vol. 28, Article ID 101668, 2022.

[209] A. P. Chowdhury and B. H. Shambharkar, "Synthesis and characterization of BiOCl–Cu2ZnSnS4 heterostructure with enhanced photocatalytic activity," *Applied Water Science*, vol. 8, no. 7, p. 202, 2018.

[210] M. K. Tiwari and P. C. Mishra, "Catalytic role of iron-superoxide dismutase in hydrogen abstraction by super oxide radical anion from ascorbic acid," *Royal Society of Chemistry Advances*, vol. 6, no. 89, pp. 86650–86662, 2016.

[211] W. He, H.-K. Kim, W. G. Wamer, D. Melka, J. H. Callahan, and J.-J. Yin, "Photogenerated charge carriers and reactive oxygen species in ZnO/Au hybrid nanostructures with enhanced photocatalytic and antibacterial activity," *Journal of the American Chemical Society*, vol. 136, no. 2, pp. 750–757, 2014.

[212] X. Zheng, J. Yuan, J. Shen et al., "A carnation-like rGO/Bi2O2CO3/BiOCl composite: efficient photocatalyst for the degradation of ciprofloxacin," *Journal of Materials Science: Materials in Electronics*, vol. 30, no. 6, pp. 5986–5994, 2019.

[213] J. Z. Y. Tan and M. M. Maroto-Valer, "A review of nanostructured non-titania photocatalysts and hole scavenging agents for CO 2 photoreduction processes," *Journal of Materials Chemistry A*, vol. 7, no. 16, pp. 9368–9385, 2019.

[214] Z. Gao and X. Qu, "Construction of ZnTiO3/Bi4NbO8Cl heterojunction with enhanced photocatalytic performance," *Nanoscale Research Letters*, vol. 15, no. 1, p. 64, 2020.

[215] I. Zelić, K. Povijač, V. Gilja, V. Tomašić, and Z. Gomzi, "Photocatalytic degradation of acetamiprid in a rotating photoreactor- determination of reactive species," *Catalysis Communications*, vol. 169, Article ID 106474, 2022.